Check for updates

ASCE

Shear Mechanism and Size Effect of RC Deep Beams without Stirrups Based on Crack Kinematics in Tests

Zhe Li[1]; Ye Li[2]; Wei-Jian Yi[3]; Yuan Huang[4]; Yun Zhou[5]; and Wang-Xi Zhang[6]

Abstract: Based on the experimental results, this paper investigates the shear mechanism of reinforced concrete deep beams without stirrups. By analyzing the kinematics of the critical shear crack, it can be found that the compression of concrete above the critical shear crack causes the crack sliding and that the combined action of the elongation of longitudinal reinforcement and the compression of concrete above the critical shear crack causes the crack opening. Based on the new-found crack kinematics and test data, the aggregate interlock force is calculated by two methods. The dowel action is also calculated. The results reveal that the shear forces transmitted by the aggregate interlock and the dowel action are relatively small, ranging from 0.5% to 9.2%. The uncracked concrete in the compression zone provides the primary resistance. Both the aggregate interlock and the uncracked concrete in the compression zone can cause a size effect. But because of the small proportion of the aggregate interlock, the size effect of shear strength is mainly caused by the size effect of uncracked concrete in the compression zone. A modified strut-and-tie model (STM) is established based on the shear mechanism found in the test. It considers the size effect using the modified size effect law. The modified STM is evaluated by comparing the calculation results with the experimental results of 194 beams. It is shown that the prediction of the modified STM is more accurate than those of the other five models, with a mean value of $V_u/V_{u,cal}$ of 1.01 and a coefficient of variation value of 0.22. The proposed model well captures the effect of the shear span-to-effective depth ratio and the size effect on the shear strength. The modified STM reflects the actual shear transfer mechanism of deep beams without stirrups and has the advantages of simple calculation and accurate prediction. **DOI: 10.1061/JSENDH.STENG-12375.**

Author keywords: Deep beam; Shear mechanism; Aggregate interlock; Strut-and-tie model; Shear strength; Size effect.

Introduction

The shear size effect phenomenon in reinforced concrete (RC) beams is represented as the decrease of the shear strength with the increase of the beam depth. Since the experimental study by Leonhardt and Walther (1962) and Kani (1967) in the 1960s, the shear size effect has been researched for decades. Based on the size effect research for slender beams (shear span-to-effective depth ratios $a/d > 2.0$–2.5) (Bažant and Kazemi 1991; Bentz 2005; Bentz and Collins 2018; Collins et al. 2015; Collins and Kuchma 1999; Daluga et al. 2018; Kani 1967; Kim and Park 1994; Korol et al. 2017; Leonhardt and Walther 1962; Lesley and Julio 2010; Lubell et al. 2004; Shioya et al. 1990), two size effect models were commonly adopted to explain it: (1) size effect law based on fracture mechanics (Bažant and Kim 1984; Bažant et al. 2007); and (2) size effect caused by aggregate interlock action (Bentz et al. 2006; Vecchio and Collins 1986). The current design codes consider the size effect of slender beams by introducing one of these two models. The size effect law based on fracture mechanics was applied to the shear model of slender beams in ACI 318-19 (ACI 2019), while the size effect model derived from the simplified modified compression field theory (SMCFT), which was based on the aggregate interlock mechanism, was introduced in CSA A23.3-14 (CSA 2014) and *fib* Model Code 2010 (CEB-FIP MC 2010). Currently, there is still an intense debate on which of these two models is more proper to consider the shear size effect. In fact, they are established based on different shear failure mechanisms. The first model believes that the compression crushing in the compression zone above the diagonal crack tip controls the maximum shear force. The second model assumes that the aggregate interlock action on the diagonal crack surfaces provides the primary shear resistance (Bažant et al. 2011; Yu et al. 2016).

As is well-known, RC deep beams without stirrups ($a/d <$ 2.0–2.5) have different shear transfer mechanisms from slender

[1]Ph.D. Candidate, College of Civil Engineering, Hunan Provincial Key Lab on Damage Diagnosis for Engineering Structures, Hunan Univ., Changsha 410082, China. ORCID: https://orcid.org/0000-0001-6593-4371. Email: zoelee@hnu.edu.cn

[2]Ph.D. Candidate, College of Civil Engineering, Hunan Provincial Key Lab on Damage Diagnosis for Engineering Structures, Hunan Univ., Changsha 410082, China. ORCID: https://orcid.org/0000-0002-9022-933X. Email: yeli@hnu.edu.cn

[3]Professor, College of Civil Engineering, Hunan Provincial Key Lab on Damage Diagnosis for Engineering Structures, Hunan Univ., Changsha 410082, China (corresponding author). Email: wjyi@hnu.edu.cn

[4]Professor, College of Civil Engineering, Hunan Provincial Key Lab on Damage Diagnosis for Engineering Structures, Hunan Univ., Changsha 410082, China. Email: huangy@hnu.edu.cn

[5]Professor, College of Civil Engineering, Hunan Provincial Key Lab on Damage Diagnosis for Engineering Structures, Hunan Univ., Changsha 410082, China. ORCID: https://orcid.org/0000-0003-3153-2467. Email: zhouyun05@hnu.edu.cn

[6]Professor, College of Civil Engineering, Hunan Provincial Key Lab on Damage Diagnosis for Engineering Structures, Hunan Univ., Changsha 410082, China. Email: wxizhang2000@hnu.edu.cn

Note. This manuscript was submitted on January 4, 2023; approved on July 19, 2023; published online on September 13, 2023. Discussion period open until February 13, 2024; separate discussions must be submitted for individual papers. This paper is part of the ***Journal of Structural Engineering***, © ASCE, ISSN 0733-9445.

beams. Other than slender beams, deep beams can redistribute the internal forces and carry an additional load after the diagonal cracks appear (Wight and MacGregor 2011). The development of diagonal cracks leads to the crack width increasing, which may reduce the contribution of aggregate interlock action to shear strength. However, the national design codes either ignore the size effect of deep beams or use the same size effect models as slender beams to consider the size effect of deep beams. Several experimental studies on the size effect of deep beams have been conducted (Birrcher et al. 2009; El-Sayed and Shuraim 2016; Li et al. 2021, 2022; Tan and Lu 1999; Tanaka et al. 2010; Walraven and Lehwalter 1994; Yang et al. 2003; Zhang and Tan 2007), but as with slender beams, there is no consensus among researchers on the size effect of deep beams. Yang et al. (2003) attributed the size effect to higher energy release by larger members. Tan and Cheng (2006) concluded that the strut geometry and boundary conditions governed the size effect of deep beams, in which the size effect of strut geometry was expressed in the form of the size effect law based on fracture mechanics. Mihaylov et al. (2013), Chen et al. (2018), and Trandafir et al. (2022) ascribed the size effect to the reduction of aggregate interlock action caused by wider diagonal crack width as the beam size increases. Hence, the size effect of deep beams needs to be further explored at experimental and theoretical levels.

Because of the existence of discontinuous regions, the section-based methods are no longer applicable. The strut-and-tie model (STM) is recommended for designing deep beams in current design codes, including ACI 318-19 (ACI 2019), AASHTO LRFD (AASHTO 2017), CSA A23.3-14 (CSA 2014), Eurocode 2 (CEN 2004), and *fib* Model Code 2010 (CEB-FIP MC 2010). To improve the accuracy of STM predicting the shear strength, many researchers have proposed various modified STMs (Brown and Bayrak 2008a, b; Chen et al. 2018; Hwang et al. 2000; Matamoros and Wong 2003; Russo et al. 2005; Tan et al. 2003, 2001; Yang and Ashour 2011; Zhang and Tan 2007), but there is still room for improvement in simultaneously meeting the requirements of simple calculation and high prediction accuracy.

In this study, the analysis of the shear mechanism and the size effect of RC deep beams without stirrups is performed on six specimens tested by the authors (Li et al. 2021, 2022). The selected six beams are large specimens with a maximum effective depth of 1,440 mm, which is rare in the shear database for deep beams without stirrups. Based on the measured crack widths in testing, the kinematic mechanism of critical shear crack, significantly affecting the generation and development of aggregate interlock, is investigated. The aggregate interlock force is calculated by two methods according to the measured crack widths and concrete strains. The dowel action is also calculated. Based on the analysis of the shear mechanism, a modified STM is established to predict the shear strength of RC deep beams without stirrups. The size effect is considered according to the actual shear mechanism observed in the tests. The accuracy of the newly modified STM and other STMs is evaluated and compared.

Analysis of Crack Kinematics

In the selected six RC deep beams without stirrups, the shear span-to-effective depth ratio a/d of four was 0.89, and that of the other two was 1.89. The heights of the six beams were 800 mm and 1,600 mm (effective depth d of 720 mm and 1,440 mm). All the test beams were monotonically loaded with a concentrated load applied at midspan. The details of the beams are listed in Table 1.

The measured crack widths at 1/4, 1/2, and 3/4 height of the beams and the longitudinal reinforcement strains were used to investigate the kinematics of the critical shear crack. As illustrated in Fig. 1, the crack widths at 1/4 height were summed and expressed as Σw_i. The elongation of longitudinal reinforcement Δl_r was calculated by integrating the longitudinal reinforcement strain along the length of the beam. The longitudinal reinforcement strains were measured both at the crack and between cracks. For RC members under tension, the crack width is generally defined as the elongation of the longitudinal reinforcement over the crack spacing on the assumption that the concrete elongation is so small that it can be ignored. However, in the actual shear test for deep beams analyzed in this study, the values of Σw_i were all greater than Δl_r, as listed in Table 2. In addition, the development of the crack widths at 1/4, 1/2, and 3/4 height of the beams in the failure span is shown in Fig. 2. The measure points of crack widths were notated in the crack pattern diagrams in Fig. 2. For example, C1-1 represents

Table 1. Summary of specimen details

Specimen ID	b (mm)	h (mm)	d (mm)	a (mm)	a/d	f_{cu} (MPa)	f_c (MPa)	f_y (MPa)	ρ (%)
D720-C35	200	800	720	640	0.89	34.7	27.4	541	1.8
D1440-C35		1,600	1,440	1,280	0.89	39.9	31.5		
D720-C50		800	720	640	0.89	51.9	41.0		
D1440-C50		1,600	1,440	1,280	0.89	54.8	43.3		
SL2_800_2		800	720	1,360	1.89	33.6	26.5		
SL2_1600_2		1,600	1,440	2,720	1.89	36.8	29.1		

Sources: Data from Li et al. (2021, 2022).
Note: f_{cu} = cubic compressive strength of concrete; and f_c = cylinder compressive strength of concrete, $0.789 f_{cu}$ according to Reineck et al. (2003).

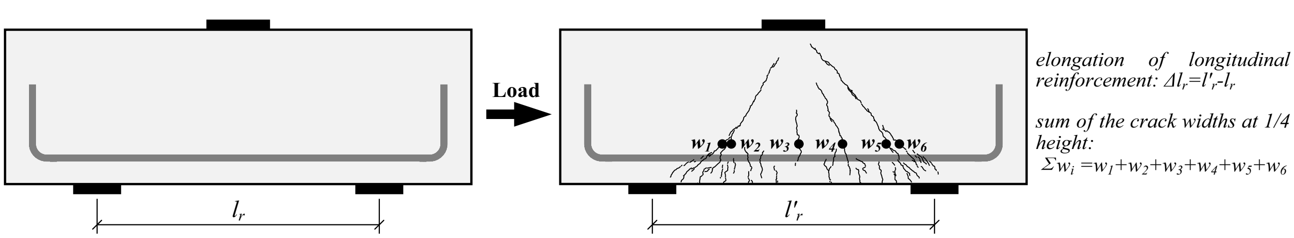

Fig. 1. Longitudinal reinforcement elongation and crack widths at 1/4 height of the beams.

Table 2. Elongation of longitudinal reinforcement and the sum of crack widths at 1/4 height of the beams

Item	D720-C35	D1440-C35	D720-C50	D1440-C50	SL2_800_2	SL2_1600_2
Δl_r (mm)	1.58	3.36	2.46	4.58	4.28	8.46
Σw_i (mm)	2.39	4.34	2.89	5.73	4.91	12.95

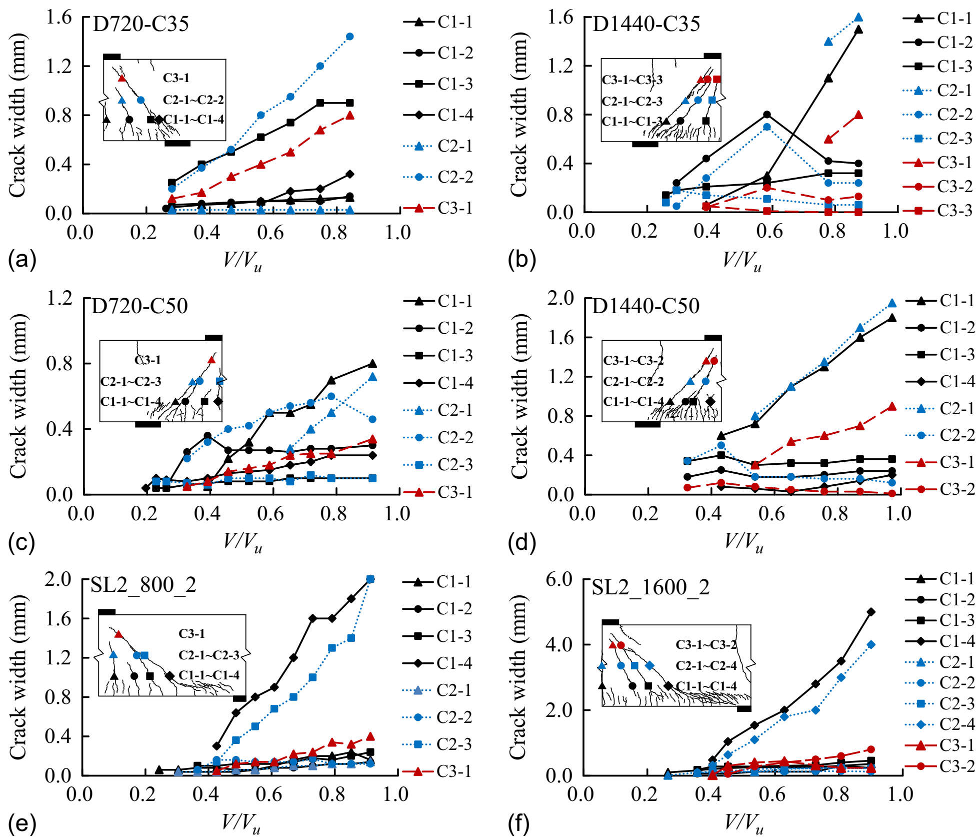

Fig. 2. Crack width against applied load: (a) D720-C35; (b) D1440-C35; (c) D720-C50; (d) D1440-C50; (e) SL2_800_2; and (f) SL2_1600_2.

the first crack width measured from left to right at the $1/4$ height of the beam. It can be seen that the width of the critical shear crack was much larger than that of other cracks. However, the elongation of the longitudinal reinforcement was nearly uniform in deep beams. It is indicated that there should be other factors causing the opening of the critical shear crack besides the elongation of the longitudinal reinforcement.

In deep beams, the applied force can be transferred from the loading point to the support by the concrete above the critical shear crack. Therefore, the concrete above the critical shear crack will be compressed and shortened. The kinematics of the critical shear crack induced by the reinforcement elongation and the concrete compression are illustrated in Fig. 3. The critical shear crack in Fig. 3 was idealized as the crack width decreases gradually along the height for ease of illustration. When there was only elongation of longitudinal reinforcement, as shown in Fig. 3(a), two opposing crack surfaces would mainly open but not slide. On the other hand, the compression of concrete above the critical shear crack caused the crack to slide and, at the same time, increased the crack width, as shown in Fig. 3(b). Generally, the practical crack kinematics was the combination of these two mechanisms. In this way, although the uncracked concrete in the compression zone prevented the sliding along the critical shear crack (Choi et al. 2007; Kotsovos 1988; Park et al. 2013; Zararis and Papadakis 2001), the aggregate interlock was still able to transfer shear force due to the compression of concrete above the critical shear crack.

Shear Transfer Mechanisms

Aggregate Interlock Force

Method 1: Aggregate Interlock Force between Two Cross Sections

According to the measurement results of the strain rosettes, the principal stresses σ_1 and σ_2 and the azimuth angle α can be obtained. The specific calculation process is given in Appendix I. In Fig. 4, arrows in the direction of strut and their vertical arrows represented the principal compressive and tensile stresses, respectively. The direction and length of the arrows indicated the direction and value of the principal stresses, respectively. As shown in Fig. 4, the directions of the principal compressive stresses at different measure points were consistent with that of the diagonal strut. It is indicated that although the crack patterns of the SL2 series and the D series differed due to their different shear span-to-effective depth ratios, the beams of the two series all directly transferred the applied load from the loading point to the support.

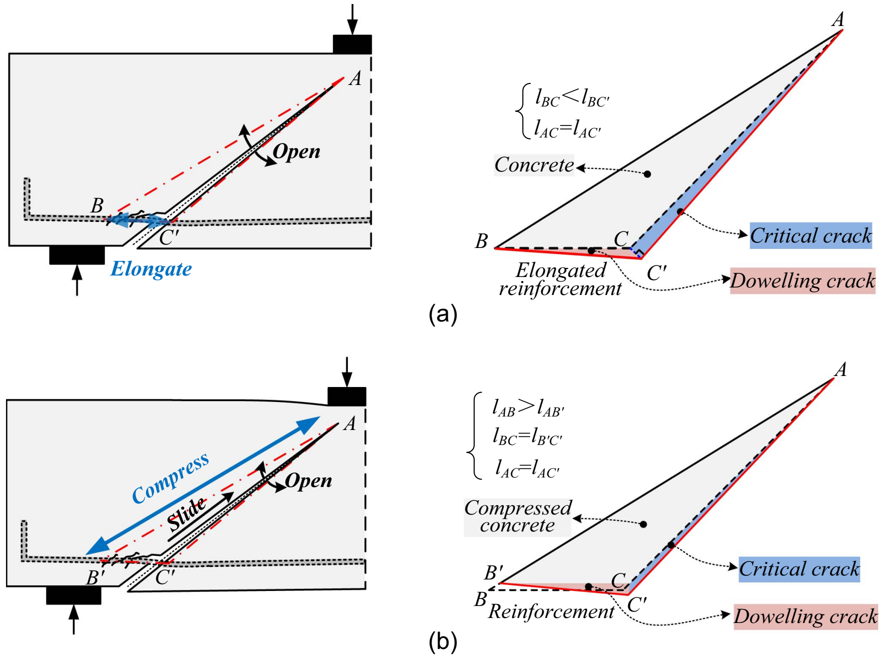

Fig. 3. Formation of crack opening and sliding: (a) crack opening due to rebar elongation; and (b) crack opening and sliding due to concrete compression.

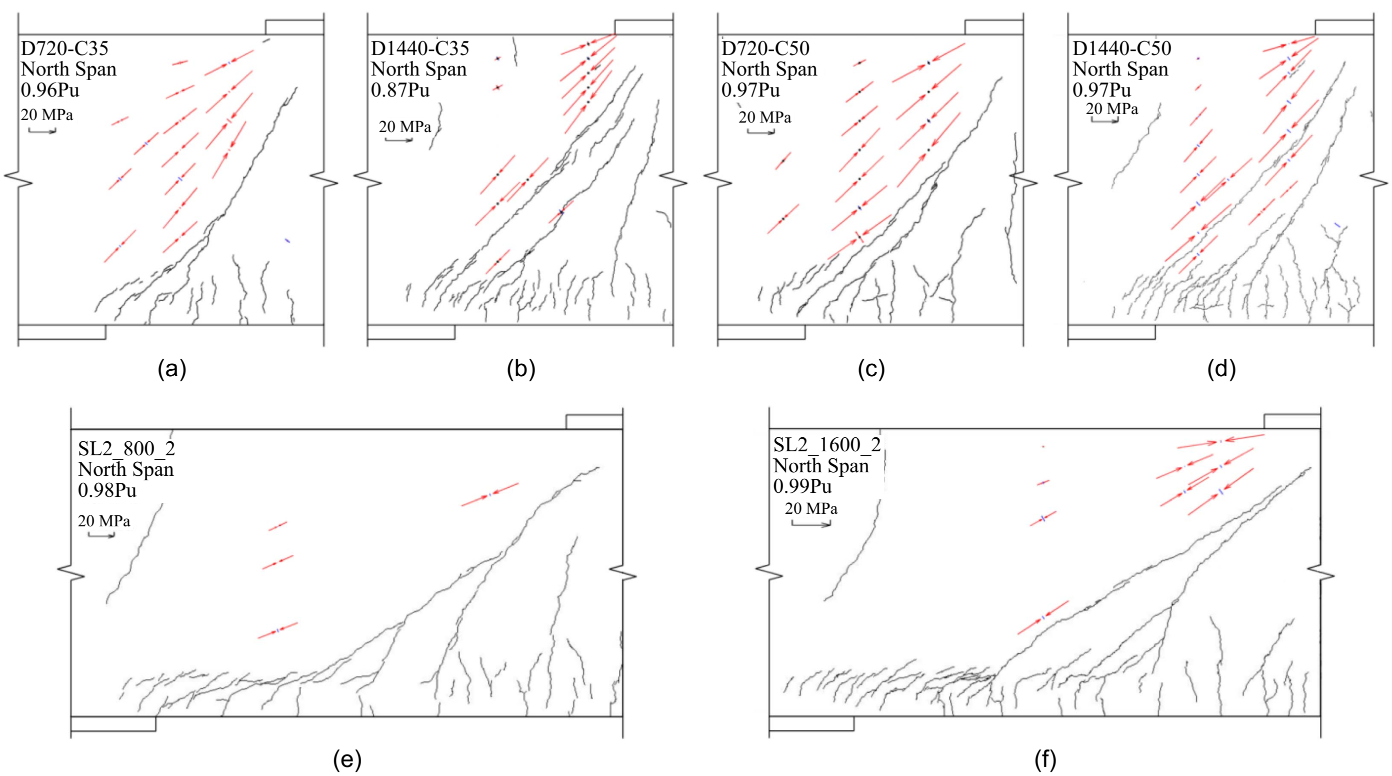

Fig. 4. Principal stress of concrete near failure: (a) D720-C35; (b) D1440-C35; (c) D720-C50; (d) D1440-C50; (e) SL2_800_2; and (f) SL2_1600_2.

The shear stress τ_m can be derived from the principal stresses σ_1 and σ_2 and the azimuth angle α, as shown in Eq. (1)

$$\tau_m = (\sigma_2 - \sigma_1) \sin\alpha \cos\alpha \tag{1}$$

Then the shear forces in the cross sections (AB and CD) $V_{cn,AB}$ and $V_{cn,CD}$ are the integral of shear stresses. The positions of cross sections AB and CD are shown in Fig. 5

$$V_{cn,AB} = b \int_{t=0}^{l_{AB}} \tau_m dt \tag{2}$$

$$V_{cn,CD} = b \int_{t=0}^{l_{CD}} \tau_m dt \tag{3}$$

The aggregate interlock force $V_{ag,BD}$ along the crack surface BD is the difference between $V_{cn,AB}$ and $V_{cn,CD}$

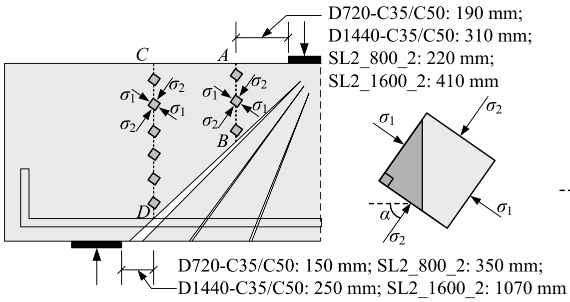

Fig. 5. Principal stresses and shear stress in the cross section of the beam.

$$V_{ag,BD} = V_{cn,CD} - V_{cn,AB} \tag{4}$$

Fig. 6 gives the development of the ratio of the shear force transmitted by the cross section to the total shear, V_{cn}/V. The curves were plotted from the occurrence of the diagonal crack BD to the beam failure.

Eq. (4) shows that the aggregate interlock force transmitted along the crack surface BD, $V_{ag,BD}$, was the difference between the shear force in the cross section AB and CD. According to the illustration of Fig. 6, there was not much difference in the shear forces transmitted by these two cross sections. The calculated values of the aggregate interlock forces of test beams are listed in Table 3. The results indicated that the mechanism of aggregate interlock had a limited contribution to the shear capacity of the test beams.

Method 2: Calculation of Aggregate Interlock Force Based on Crack Kinematics

The theoretical model Walraven (1980) built was used to evaluate the aggregate interlock between crack surfaces. It was referred to as a two-phase model in which the aggregate particles were simplified as a rigid sphere, and the cement matrix was idealized as rigid-plastic material. The interlock forces were created in the contact areas between aggregate particles and the cement matrix. For ease of calculation, Walraven put forward an empirical model based on the regression of the test results called

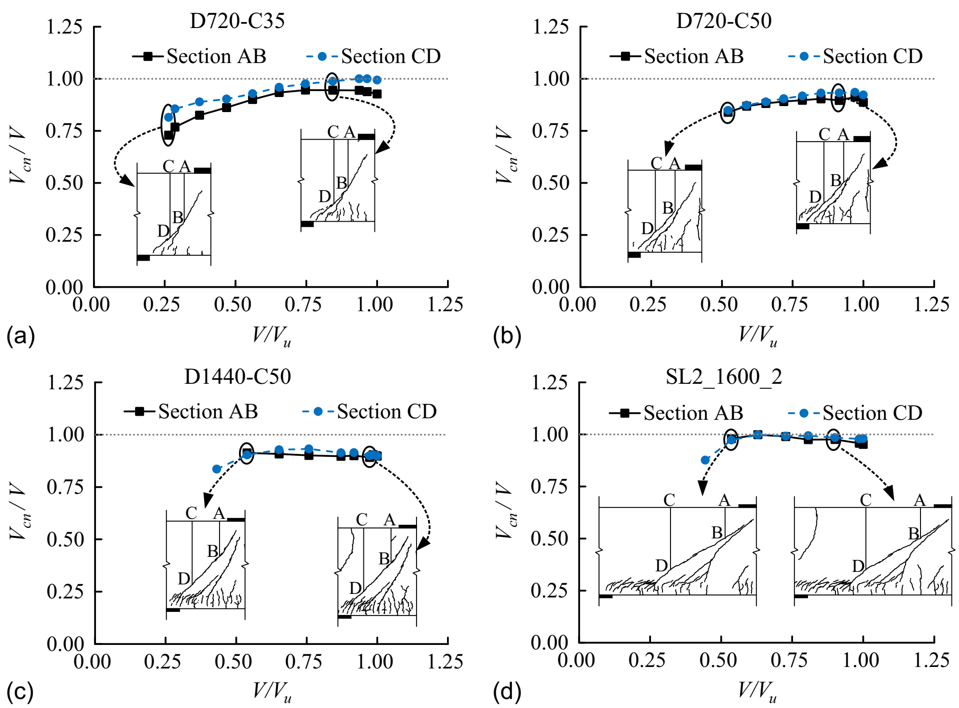

Fig. 6. Shear force transmitted by the cross section under different load levels: (a) D720-C35; (b) D720-C50; (c) D1440-C50; and (d) SL2_1600_2.

Table 3. Contribution of the aggregate interlock and dowel action to the shear capacity

			Aggregate interlock				Dowel action	
			Method 1		Method 2			
Specimen ID	V_u (kN)	$V_u/(bdf_c)$	$V_{ag,1}$ (kN)	$V_{ag,1}/V_u$	$V_{ag,2}$ (kN)	$V_{ag,2}/V_u$	V_d (kN)	V_d/V_u
D720-C35	802	0.204	53.7	6.7%	53.6	6.7%	16.6	2.5%
D1440-C35	1544	0.170	—	—	36.6	2.4%	24.2	1.8%
D720-C50	1149	0.195	41.3	3.6%	64.1	5.6%	3.1	0.3%
D1440-C50	1851	0.149	0.0	0.0%	0.0	0.0%	9.9	0.5%
SL2_800_2	493	0.134	—	—	2.6	0.5%	3.9	0.9%
SL2_1600_2	837	0.104	23.4	2.8%	0.0	0.0%	8.2	1.1%

Note: V_u is the ultimate shear strength of beams; "—" means that the aggregate interlock force of D1440-C35 and SL2_800_2 could not be calculated by Method 1 due to several concrete strain rosettes at section AB or CD being damaged during the loading process (see Fig. 4).

J. Struct. Eng., 2023, 149(11): 04023159

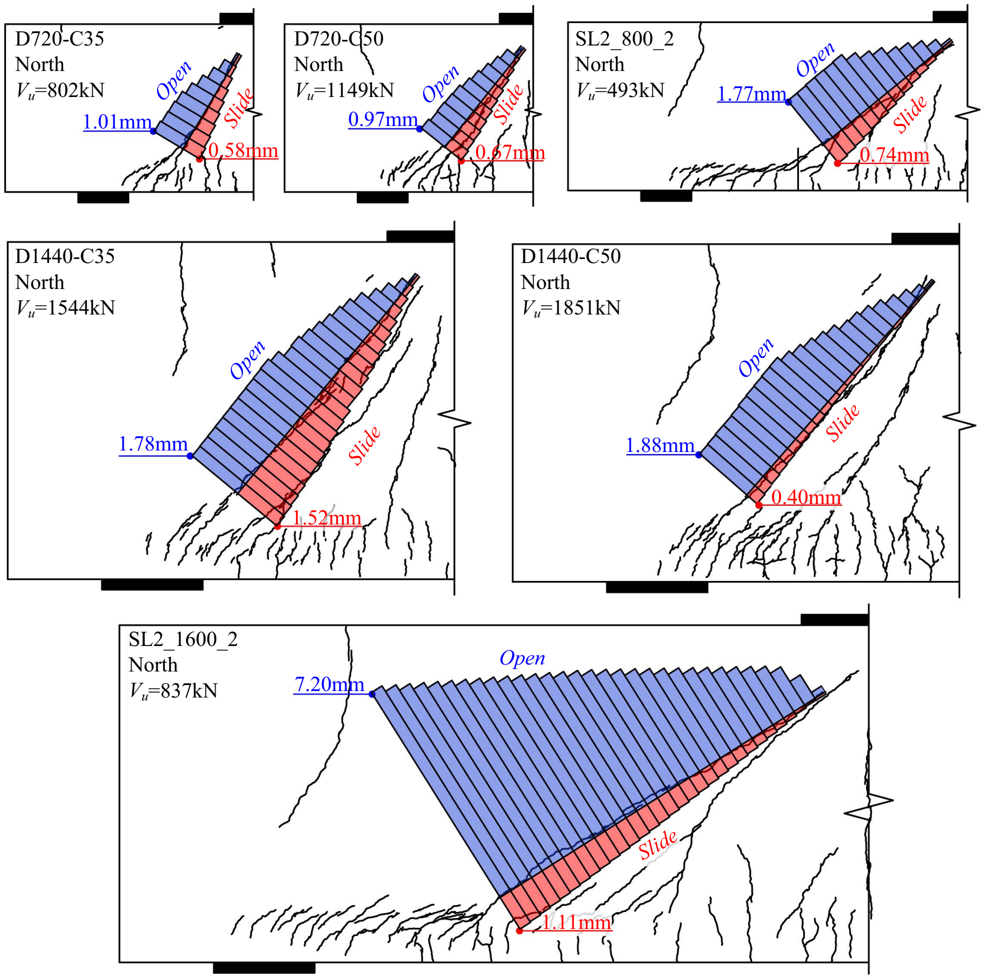

Fig. 7. Crack opening and crack sliding of each segment.

the linear aggregate interlock model. The equations of this model are expressed as

$$\tau_{ag} = -\frac{f_{cu}}{30} + [1.8w^{-0.8} + (0.234w^{-0.707} - 0.2)f_{cu}]s \quad (\tau_{ag} \geq 0) \tag{5}$$

$$\sigma_{ag} = -\frac{f_{cu}}{20} + [1.35w^{-0.63} + (0.191w^{-0.552} - 0.15)f_{cu}]s \quad (\sigma_{ag} \geq 0) \tag{6}$$

where σ_{ag} and τ_{ag} = normal and shear stress on the crack surface due to the aggregate interlock, respectively; w = crack width, representing the opening of the crack; and s = crack sliding, meaning the parallel movement of crack surfaces.

The values of crack widths w at the ultimate shear strength V_u were obtained by the linear extrapolation of crack widths measured by a hand-held micrometer before failure. Strain rosettes were applied on both sides of the critical shear crack to measure the concrete compressive strains. The difference in the concrete compression deformation between the two surfaces of the critical shear crack was the crack sliding s. The whole critical shear crack was divided into several segments. The length of each segment was about three times the maximum aggregate size ($3d_{ag} \approx 60$ mm), which could reflect the material characteristics of concrete as an anisotropic material and correspond to the length of the concrete strain gauges. The crack opening w and sliding s of each segment were drawn in Fig. 7, and blue and red strips represent the crack opening and sliding, respectively. Fig. 7 shows that the crack opening increases significantly as the beam size increases.

Introducing the values of crack width w and crack sliding s into Eqs. (5) and (6), the normal stress σ_{ag} and shear stress τ_{ag} can be determined. After that, the aggregate interlock force V_{ag} can be calculated as the following expression:

$$V_{ag} = b\left(\int_{t=0}^{l_c} \tau_{ag} \sin\alpha_c(t)dt - \int_{t=0}^{l_c} \sigma_{ag} \cos\alpha_c(t)dt\right) \tag{7}$$

where l_c = length of the whole critical shear crack; and $\alpha_c(t)$ = inclination angle of each crack segment.

The aggregate interlock forces of the test beams are listed in Table 3. It can be seen that the contribution to the shear capacity by aggregate interlock ranges from 0% to 6.7%.

Dowel Action

The equation put forward by Chen et al. (2018) was used to calculate the dowel action of longitudinal reinforcement

$$V_d = \left(1 - \frac{\sigma_{sc}}{f_y}\right)\frac{n_b d_b^3 f_y}{3l_{de}} \tag{8}$$

where f_y = yield stress of the longitudinal tension bar; σ_{sc} = tensile stress in longitudinal reinforcement; d_b = diameter of longitudinal

J. Struct. Eng., 2023, 149(11): 04023159

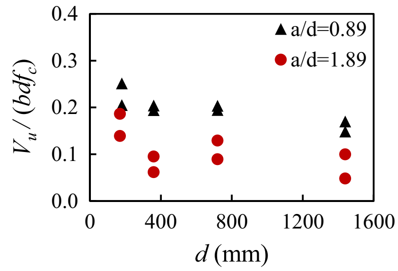

Fig. 8. Normalized shear strength versus effective depth.

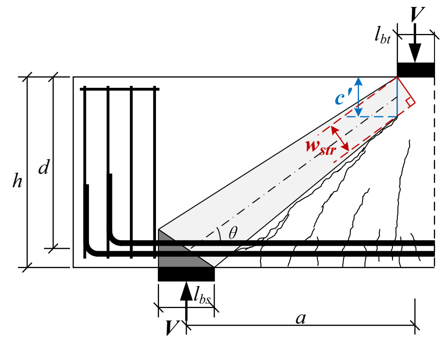

Fig. 9. Configuration of modified STM.

reinforcement; n_b = number of longitudinal reinforcements; and l_{de} = length of delamination crack.

Table 3 lists the results of the dowel action of longitudinal reinforcement. The contribution of dowel action to shear capacity can be seen as insignificant. The largest proportion of it was 2.5% for D720-C35.

Moreover, in Method 1, the difference between applied shear force and $V_{cn,CD}$ (shear transferred by cross section CD) was regarded as the shear force carried by the dowel action of longitudinal reinforcement. As shown in Fig. 6, the dowel action mechanism started to play a role after the critical shear crack appeared, and the contribution of dowel action to shear capacity was small. Besides, with the propagation of the dowelling cracks along the longitudinal reinforcement, the dowel action decreased as the applied load increased.

As the presented calculation results show, the aggregate interlock and the dowel action contributions to shear strength were less than 6.7% and 2.5%, respectively. It can be concluded that the shear forces transmitted by the aggregate interlock and dowel action of longitudinal reinforcement were relatively small. Therefore, the uncracked concrete in the compression zone provided the majority of the resistance. Test data from 16 specimens were collected from the authors' work (Li et al. 2021, 2022), including specimens with an effective depth of less than 0.2–0.25 m for which almost no size effect was observed (Chen et al. 2018; Yu et al. 2016). Fig. 8 shows that the normalized shear strength $V_u/(bdf_c)$ of these specimens generally decreases with the increase of the effective depth. In Table 3, as the beam height increased from 800 mm to 1,600 mm, for the beams with a/d of 0.89, $V_u/(bdf_c)$ decreased by 16.7% and 23.6% for the beams with a design concrete strength of 35 and 50 MPa, respectively. For the beams with a/d of 1.89, $V_u/(bdf_c)$ decreased by 22.4%. The test results showed a pronounced size effect. The aggregate interlock force decreased with the increase in beam height, as shown in Table 3, indicating that the aggregate interlock can cause the size effect. However, because the proportion of the aggregate interlock was small, the size effect of shear strength was mainly caused by the size effect of the uncracked concrete in the compression zone.

Calculation Model of Shear Capacity

Modified STM Model

According to the presented experimental analysis, the present study proposed a modified STM, which considered that the shear strength of RC deep beams without stirrups was mainly carried by the uncracked concrete in the compression zone. It can be expressed as the following equation:

$$V = \phi\eta F_{str}\sin\theta = \phi\eta\kappa\xi f_c w_{str} b\sin\theta \tag{9}$$

where φ = strength reduction coefficient taken as 1.0 because the model in this paper focuses on the precision of prediction rather than the safety; F_{str} = ultimate resultant force in the strut; and η = coefficient that takes account of the contribution of aggregate interlock and dowel action of longitudinal reinforcement to shear capacity. According to the presented test results, the shear force transmitted by the aggregate interlock and dowel action is assumed as $5\%V$, so η is taken as 1.05. κ is the brittleness coefficient of concrete, $\kappa = 1 - f_c/200$.

ξ is the size effect factor. As discussed, the size effect of shear strength was mainly caused by the size effect of the uncracked concrete in the compression zone. Therefore, ξ is expressed as an equation related to the width of the top of the uncracked concrete strut w_{str} (Fig. 9). Also, ξ is defined to have the form of modified size effect law put forward by Kim and Eo (1990), which was added a size-independent part to Bažant's size effect law

$$\xi = \frac{C_1}{\sqrt{1 + w_{str}/(2d_{ag})}} + C_2 \tag{10}$$

where $2d_{ag}$ = width of the crack band (Bažant 1984). The existing test data showed little effect on the width of the crack band for the aggregate size usually used in construction (Kim and Eo 1990). So $2d_{ag}$ can be taken as constant, equaling 38 mm in this paper. C_1 and C_2 are undetermined parameters, which are determined based on test results. The width of the top of the uncracked concrete strut w_{str} is expressed as

$$w_{str} = c'\cos\theta \tag{11}$$

where θ = angle between the center line of the strut and the horizontal direction, $\theta = \arctan[(d - 0.5c')/(a - 0.5l_{bt})]$; c' = depth of the uncracked concrete at the edge of the loading plate, as shown in Figs. 9 and 10.

When the critical shear crack arrives at the position of the flexural neutral axis (point A in Fig. 10), the depth of the compression zone is c. Then, with the load increase, the critical shear crack will further develop and enter the underside of the loading plate before failure, as shown in Fig. 10. According to Zhang and Tan (2007), the shear size effect was related to the loading plate size. Moreover, per the discovery found by Mihaylov et al. (2010) and Trandafir et al. (2022), the dimension of the critical loading zone (CLZ), which was the concrete near the edge of the loading plate above the diagonal crack, was determined by the loading plate width and the diagonal crack angle near the loading plate. Choi et al. (2007) also revealed that the depth of the uncracked concrete was proportional to the depth of the compression zone c and decreased with the increase of the shear span-to-effective depth ratio a/d. Therefore, c' is related to the loading plate width l_{bt} and the shear

J. Struct. Eng., 2023, 149(11): 04023159

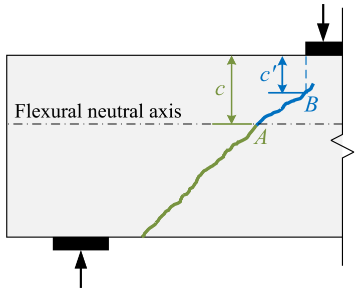

Fig. 10. Crack propagation of the deep beams.

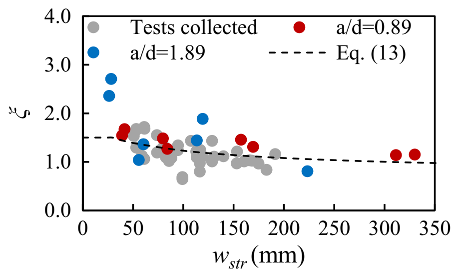

Fig. 11. Size effect factor ξ versus uncracked concrete strut width w_{str}.

span-to-effective depth ratio a/d. Additionally, c' is proportional to c, where the influence of the stiffness of the longitudinal reinforcement is reflected in c. In this way, the equation has the potential to extend to other materials of longitudinal reinforcement, such as fiber-reinforced polymer (FRP) bars (Tureyen and Frosch 2003). Therefore, the expression of c', which contains three parameters, a/d, l_{bt}/d, and c, is assumed to be Eq. (12), where C_3 and C_4 are undetermined parameters

$$c' = C_3\left(\frac{a - 0.5l_{bt}}{d}\right)^{C_4} c \tag{12}$$

where $c \approx 0.75(n\rho)^{1/3}d$ (Cladera et al. 2017); n = ratio of the steel elastic modulus to the concrete elastic modulus, $n = E_s/E_c$; E_c is taken as $4{,}700\sqrt{f_c}$ (ACI 2019); E_s is taken as 200 GPa; and ρ = ratio of the longitudinal reinforcement.

A total of 55 deep beams were collected from the experimental study on size effect by Li et al. (2021, 2022), Yang et al. (2003), Zhang and Tan (2007), and El-Sayed and Shuraim (2016), in which the effective depth d of the beams ranged from 170 to 1,440 mm and the shear span-to-depth ratio a/d of the beams ranged from 0.9 to 1.9. The undetermined parameters can be obtained through the nonlinear regression analysis of the 55 beams: $C_1 = 1.2$, $C_2 = 0.6$, $C_3 = 0.72$, $C_4 = -3/4$. Consequently, Eqs. (10) and (12) become

$$\xi = \frac{1.2}{\sqrt{1 + w_{str}/38}} + 0.6 \tag{13}$$

$$c' = 0.72\left(\frac{a - 0.5l_{bt}}{d}\right)^{-\frac{3}{4}} c = 0.54\left(\frac{a - 0.5l_{bt}}{d}\right)^{-\frac{3}{4}} (n\rho)^{\frac{1}{3}} d \tag{14}$$

Substituting Eq. (14) into Eq. (11), w_{str} is obtained. The shear force can be calculated by substituting Eqs. (11) and (13) into Eq. (9).

Based on the test data of V_u in the authors' work (Li et al. 2021, 2022) and collected from other size effect studies (Yang et al. 2003; Zhang and Tan 2007; El-Sayed and Shuraim 2016), the size effect factor ξ was further validated by Eq. (15). The calculation results are shown in Fig. 11

$$\xi = \frac{V_u}{\eta\kappa f_c w_{str} b \sin\theta} \tag{15}$$

In Fig. 11, the red and blue points represent the studies by authors, which contain the specimens analyzed in this paper. The gray points are test results collected from other studies. Because there is almost no size effect for beams with an effective depth of less than 0.2 m, the w_{str} corresponding to this effective depth range is about 30 mm. So the upper limit of Eq. (13) is defined as 1.5. When $\xi > 1.5$, take it as 1.5. As shown in Fig. 11, the trend of ξ calculated by Eq. (13) agrees with that of ξ obtained from test data.

Model Verification

A total of 127 specimens with $a/d \leq 2$ were selected from Reineck's database of the RC deep beams without stirrups (Reineck and Todisco 2014) after filtering out the specimens without loading plates and bearing plates. Moreover, according to the experimental research by Walraven and Lehwalter (1994), Yang et al. (2003), Zhang and Tan (2007), Tanaka et al. (2010), Mihaylov et al. (2010), El-Sayed and Shuraim (2016), and Li et al. (2021, 2022), 67 additional specimens were added in the database. Therefore, a database containing 194 RC deep beams without stirrups was established. The test parameters of specimens in the established database are described in Appendix II. The test results of all specimens in the database were compared with the predicted shear strength by modified STM and the other five models proposed by Russo et al. (2005), Zhang and Tan (2007), Choi et al. (2007), Yang and Ashour (2011), and Mihaylov et al. (2013). In addition to Russo's model, the other four models take into account the size effect. The shear strength ratios $V_u/V_{u,cal}$ calculated by the modified STM are listed in Appendix II. Statistical results, including the mean value, the standard deviation (SD), and the coefficient of variation (COV) of the shear strength ratio $V_u/V_{u,cal}$, are given in Table 4. In addition, Fig. 12 gives the value $V_u/V_{u,cal}$ versus the shear span-to-depth ratio a/d and effective depth d, respectively. The modified STM proposed in this paper shows the most accurate prediction with a mean value of $V_u/V_{u,cal}$ of 1.01 and a COV value of 0.22. Moreover, as shown in Fig. 12, the trend line of the $V_u/V_{u,cal}$ in the proposed model is almost horizontal as the a/d and effective depth d increase, while the trend lines of the other models show upward or downward trends. It is indicated that the influences of the shear

Table 4. Statistical results of experimental-to-predicted shear strength ratio

Statistical results	Proposed model Eq. (9)	Russo et al. (2005)	Zhang and Tan (2007)	Choi et al. (2007)	Yang and Ashour (2011)	Mihaylov et al. (2013)
Mean	1.01	0.99	1.03	0.87	1.45	0.95
SD	0.22	0.26	0.28	0.24	0.48	0.25
COV	0.22	0.26	0.27	0.28	0.33	0.27

J. Struct. Eng., 2023, 149(11): 04023159

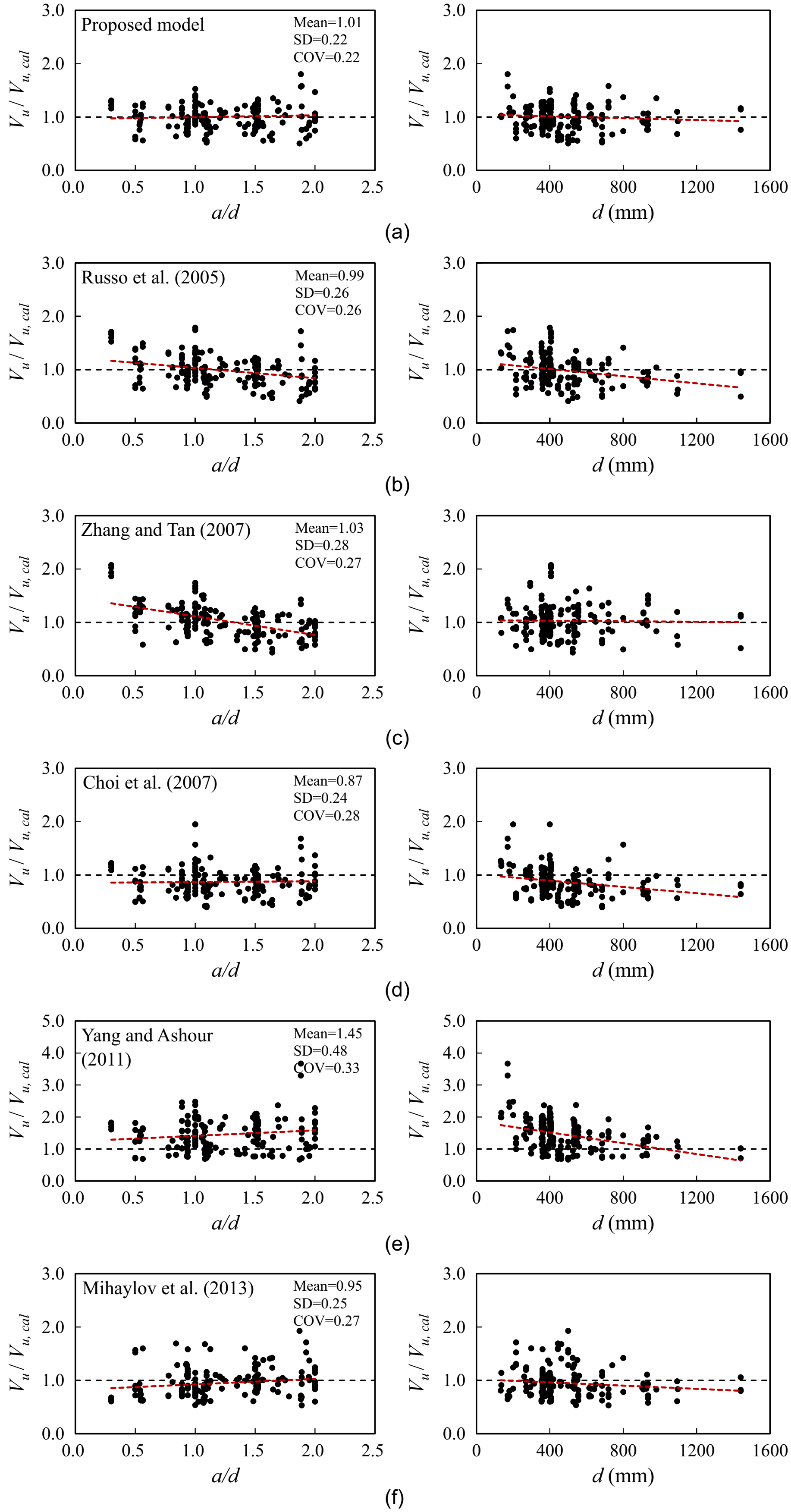

Fig. 12. Shear strength predictions for test beams by different models: (a) proposed model; (b) Russo et al. (2005); (c) Zhang and Tan (2007); (d) Choi et al. (2007); (e) Yang and Ashour (2011); and (f) Mihaylov et al. (2013).

span-to-depth ratio and the effective depth are well considered in the proposed model.

Conclusions

This paper made a deep analysis of six RC deep beams without stirrups. The shear mechanism and the size effect of RC deep beams without stirrups were investigated based on the test results. A modified STM was established. The model's accuracy was evaluated and compared with the other five models. The following conclusions can be made in this paper:

1. Based on the measured crack widths, the kinematic mechanism of the critical shear crack was studied. It can be found that the crack sliding was caused by the compression of concrete above the critical shear crack. The crack opening was caused by the combined action of the elongation of longitudinal reinforcement and the compression of concrete above the critical shear crack.
2. Different methods were used to calculate the contributions of the aggregate interlock and the dowel action to the shear capacity of the test beams. It revealed that the shear forces transmitted through aggregate interlock and dowel action were relatively small. The uncracked concrete in the compression zone provided the primary resistance for RC deep beams without stirrups. Even though the aggregate interlock could cause the size effect, the proportion of the aggregate interlock was small. Therefore, the size effect of shear strength was mainly caused by the size effect of the uncracked concrete in the compression zone.
3. The modified STM was established based on the shear mechanism found in the test, reflecting the major contribution of uncracked concrete in the compression zone. The modified STM considered the size effect of deep beams by using the modified size effect law based on fracture mechanics.
4. A database containing 194 RC deep beams without stirrups was established in this paper. The modified STM was evaluated by comparing the calculation results with the experimental results in the database. Compared to the other five models, the modified STM provided the most accurate prediction with a mean value of $V_u/V_{u,cal}$ of 1.01 and a COV value of 0.22. Moreover, the influences of the shear span-to-depth ratio and the effective depth were well considered in the proposed model. Therefore, the modified STM reflected the actual shear mechanism of deep beams without stirrups and had the advantages of simple calculation and accurate prediction.

Appendix I. Calculation of the Principal Stresses $\boldsymbol{\sigma_1}$ and $\boldsymbol{\sigma_2}$ for Section "Method 1"

The principal strains ε_1 and ε_2, as well as the azimuth angle α, can be computed by Eqs. (16) and (17)

$$\tan 2\alpha = -\frac{\gamma_{xy}}{\varepsilon_x - \varepsilon_y} \tag{16}$$

$$\left.\begin{matrix}\varepsilon_1\\ \varepsilon_2\end{matrix}\right\} = \frac{\varepsilon_x + \varepsilon_y}{2} \pm \sqrt{\left(\frac{\varepsilon_x - \varepsilon_y}{2}\right)^2 + \left(\frac{\gamma_{xy}}{2}\right)^2} \tag{17}$$

where $\varepsilon_x = \varepsilon_{0°}$; $\varepsilon_y = \varepsilon_{90°}$; $\gamma_{xy} = \varepsilon_{0°} + \varepsilon_{90} - \circ\varepsilon_{45°}$, as shown in Fig. 13.

Under the situation of knowing the principal strains ε_1 and ε_2 through the method aforementioned, the two-dimensional damage constitutive model of concrete proposed by Li and Ren (2009) was used to calculate the principal stresses σ_1 and σ_2. From the test

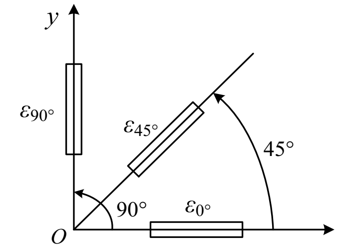

Fig. 13. Strain rosette formation.

results, the principal strains were small, so strain and stress were regarded as elastic relationships. Therefore, biaxial strain-stress relation in effective stress space is expressed as

$$\begin{Bmatrix}\bar{\sigma}_1\\ \bar{\sigma}_2\end{Bmatrix} = \frac{E}{1-\nu^2}\begin{bmatrix}1 & \nu\\ \nu & 1\end{bmatrix}\begin{Bmatrix}\varepsilon_1\\ \varepsilon_2\end{Bmatrix} \tag{18}$$

According to the principle of strain equivalence (Lemaitre 1971), the relation between nominal stress tensor (also known as Cauchy stress) $\boldsymbol{\sigma}$ and effective stress tensor $\bar{\boldsymbol{\sigma}}$ is defined as follows under biaxial stress state

1. T-T region ($\bar{\sigma}_1 > 0, \bar{\sigma}_2 \geq 0$)

$$\begin{Bmatrix}\sigma_1\\ \sigma_2\end{Bmatrix} = [1 - d_t(\varepsilon_{t,e})]\begin{Bmatrix}\bar{\sigma}_1\\ \bar{\sigma}_2\end{Bmatrix} \tag{19}$$

2. C-C region ($\bar{\sigma}_1 \leq 0, \bar{\sigma}_2 < 0$)

$$\begin{Bmatrix}\sigma_1\\ \sigma_2\end{Bmatrix} = [1 - d_c(\varepsilon_{c,e})]\begin{Bmatrix}\bar{\sigma}_1\\ \bar{\sigma}_2\end{Bmatrix} \tag{20}$$

3. T-C region ($\bar{\sigma}_1 \geq 0, \bar{\sigma}_2 < 0$)

$$\begin{Bmatrix}\sigma_1\\ \sigma_2\end{Bmatrix} = \begin{bmatrix}[1 - d_t(\varepsilon_{t,e})] & 0\\ 0 & [1 - d_c(\varepsilon_{c,e})]\end{bmatrix}\begin{Bmatrix}\bar{\sigma}_1\\ \bar{\sigma}_2\end{Bmatrix} \tag{21}$$

where d_t and d_c = tensile damage scalar and compressive damage scalar, respectively, and the expression is defined as [GB50010-2010 (China Architectural and Building Press 2010)]

$$d_t(\varepsilon_{t,e}) = \begin{cases}1 - \rho_t[1.2 - 0.2x_t^5] & x_t \leq 1\\ 1 - \dfrac{\rho_t}{\alpha_t(x_t-1)^{1.7} + x_t} & x_t > 1\end{cases} \tag{22}$$

$$d_c(\varepsilon_{c,e}) = \begin{cases}1 - \dfrac{\rho_c n}{n - 1 + x_c^n} & x_c \leq 1\\ 1 - \dfrac{\rho_c}{\alpha_c(x_c-1)^2 + x_c} & x_c > 1\end{cases} \tag{23}$$

where $\rho_t = f_t/(E_c\varepsilon_t)$; $x_t = \varepsilon_{t,e}/\varepsilon_t$; $\alpha_t = 0.312f_t^2$; $\rho_c = f_c/(E_c\varepsilon_c)$; $n = E_c\varepsilon_c/(E_c\varepsilon_c - f_c)$; $x_c = \varepsilon_{c,e}/\varepsilon_c$; $\alpha_c = 0.157f_c^{0.785} - 0.905$; f_t and f_c = uniaxial tensile strength and uniaxial compressive strength of concrete cylinder, respectively; ε_t and ε_c = tensile peak strain and compressive peak strain corresponding to f_t and f_c, respectively.

Double damage scalars d_t and d_c are aimed at stimulating the different mechanical characteristics of concrete in tension and compression. They are functions of energy equivalent strains $\varepsilon_{t,e}$ or $\varepsilon_{c,e}$ [Eqs. (22) and (23)], which are the bridges between the multidimensional stress state and the one-dimensional stress state. The derivation of energy equivalent strain is described in detail hereafter.

J. Struct. Eng., 2023, 149(11): 04023159

In the effective stress space, the damage energy release rates (DERR) Y^+ and Y^- are proposed as (Wu et al. 2006)

$$Y^+ = \frac{1}{2E_0}\left[\frac{2(1+\nu_0)}{3}3\bar{J}_2^+ + \frac{1-2\nu_0}{3}(\bar{I}_1^+)^2 - \nu_0\bar{I}_1^+\bar{I}_1^-\right] \tag{24}$$

$$Y^- = \frac{1}{2b_0}\left(\alpha\bar{I}_1^- + \sqrt{3\bar{J}_2^-}\right)^2 \tag{25}$$

Based on the hypothesis of the damage consistent condition (Li and Ren 2009), the energy equivalent strain ε_e could be obtained by solving the following equation:

$$Y^{\pm}(\varepsilon_1, \varepsilon_2) = Y_1^{\pm}(\varepsilon_e) \tag{26}$$

Combining the Eqs. (24)–(26) and the biaxial strain-stress relation prescribed in Eq. (18), the energy equivalent strains $\varepsilon_{t,e}$ and $\varepsilon_{c,e}$ under different tension-compression states are given

1. T-T region ($\bar{\sigma}_1 > 0, \bar{\sigma}_2 \geq 0$)

$$\varepsilon_{t,e} = \sqrt{\frac{1}{1-\nu^2}[(\varepsilon_1)^2 + (\varepsilon_2)^2 + 2\nu\varepsilon_1\varepsilon_2]} \tag{27}$$

2. C-C region ($\bar{\sigma}_1 \leq 0, \bar{\sigma}_2 < 0$)

$$\varepsilon_{c,e} = \frac{1}{(1-\nu^2)(\alpha_s - 1)}\Big[\alpha_s(1+\nu)(\varepsilon_1+\varepsilon_2) + \sqrt{(\varepsilon_1+\nu\varepsilon_2)^2 + (\varepsilon_2+\nu\varepsilon_1)^2 - (\varepsilon_1+\nu\varepsilon_2)(\varepsilon_2+\nu\varepsilon_1)}\Big] \tag{28}$$

$$\alpha_s = \frac{f_{bc} - f_c}{2f_{bc} - f_c} \tag{29}$$

where f_{bc} = equibiaxial compressive strength, the ratio of f_{bc}/f_c generally ranges from 1.16 to 1.20 based on experimental data.

3. T-C region ($\bar{\sigma}_1 \geq 0, \bar{\sigma}_2 < 0$)

$$\varepsilon_{t,e} = \sqrt{\frac{1}{1-\nu^2}\varepsilon_1(\varepsilon_1+\nu\varepsilon_2)} \tag{30}$$

$$\varepsilon_{c,e} = \frac{1}{(1-\nu^2)(\alpha_s - 1)}\Big[\alpha_s(1+\nu)(\varepsilon_1+\varepsilon_2) + \sqrt{(\varepsilon_1+\nu\varepsilon_2)^2 + (\varepsilon_2+\nu\varepsilon_1)^2 - (\varepsilon_1+\nu\varepsilon_2)(\varepsilon_2+\nu\varepsilon_1)}\Big] \tag{31}$$

Appendix II. Shear Database of RC Deep Beams without Stirrups

No.	Authors and reference	Specimen	b (mm)	h (mm)	d (mm)	a (mm)	a/d	f_c (MPa)	ρ (%)	l_{bt} (mm)	d_{ag} (mm)	V_u (kN)	$V_u/V_{u.cal}$
1	Clark (1951)	BO-1	203.2	457.2	391.2	762.0	1.95	23.6	0.98	88.9	NR	122.2	0.843
2		BO-2	203.2	457.2	390.4	762.0	1.95	23.9	0.98	88.9	NR	95.4	0.654
3		BO-3	203.2	457.2	390.2	762.0	1.95	23.5	0.98	88.9	NR	129.2	0.897
4		CO-1	203.2	457.2	390.9	609.6	1.56	24.7	0.98	88.9	NR	175.7	0.893
5		CO-3	203.2	457.2	390.5	609.6	1.56	23.6	0.98	88.9	NR	168.3	0.886
6		DO-1	203.2	457.2	390.5	457.2	1.17	25.9	0.98	88.9	NR	223.1	0.812
7		DO-3	203.2	457.2	390.9	457.2	1.17	26.0	0.98	88.9	NR	224.8	0.816
8	Moody et al. (1954)	III-24a	177.8	609.6	533.4	812.8	1.52	17.8	2.72	203.2	25.4	297.9	1.220
9		III-24b	177.8	609.6	533.4	812.8	1.52	20.6	2.72	203.2	25.4	304.6	1.112
10		III-25a	177.8	609.6	533.4	812.8	1.52	24.3	3.45	203.2	25.4	269.0	0.818
11		III-25b	177.8	609.6	533.4	812.8	1.52	17.2	3.45	203.2	25.4	291.2	1.154
12		III-26a	177.8	609.6	533.4	812.8	1.52	21.7	4.25	203.2	25.4	422.5	1.333
13		III-26b	177.8	609.6	533.4	812.8	1.52	20.6	4.25	203.2	25.4	398.0	1.304
14		III-27a	177.8	609.6	533.4	812.8	1.52	21.4	2.72	203.2	25.4	349.1	1.241
15		III-27b	177.8	609.6	533.4	812.8	1.52	22.9	2.72	203.2	25.4	358.0	1.207
16		III-28a	177.8	609.6	533.4	812.8	1.52	23.3	3.34	203.2	25.4	304.6	0.964
17		III-28b	177.8	609.6	533.4	812.8	1.52	22.4	3.34	203.2	25.4	342.4	1.115
18		III-29a	177.8	609.6	533.4	812.8	1.52	21.7	4.25	203.2	25.4	391.3	1.231
19		III-29b	177.8	609.6	533.4	812.8	1.52	25.0	4.25	203.2	25.4	438.0	1.244
20	Morrow and Viest (1957)	B14 B2	304.8	406.4	368.3	444.5	1.21	14.6	1.89	177.8	25.4	367.9	1.130
21		B14 A4	304.8	406.4	362.0	444.5	1.23	22.6	2.54	177.8	25.4	512.4	1.074
22		B14 B4	304.8	406.4	368.3	444.5	1.21	26.3	1.89	177.8	25.4	501.3	0.984
23		B14 A6	304.8	406.4	355.6	444.5	1.25	45.4	3.91	177.8	25.4	901.6	1.086
24		B21 B2	304.8	406.4	366.8	622.3	1.70	13.9	1.90	177.8	25.4	239.2	1.129
25		B21 A4	304.8	406.4	368.3	622.3	1.69	29.8	2.50	177.8	25.4	523.8	1.283
26		B21 B4	304.8	406.4	368.3	622.3	1.69	27.1	1.89	177.8	25.4	397.1	1.115
27		B21 A6	304.8	406.4	355.6	622.3	1.75	45.3	3.91	177.8	25.4	579.4	1.035
28	Watstein and Mathey (1958)	B-18-1	203.2	457.2	403.9	609.6	1.51	25.4	2.99	88.9	25.4	311.4	1.097
29		B-18-2	203.2	457.2	403.9	609.6	1.51	23.0	2.99	88.9	25.4	309.1	1.173
30		C-18-1	203.2	457.2	403.9	609.6	1.51	25.6	1.85	88.9	25.4	289.1	1.141

No.	Authors and reference	Specimen	b (mm)	h (mm)	d (mm)	a (mm)	a/d	f_c (MPa)	ρ (%)	l_{bt} (mm)	d_{ag} (mm)	V_u (kN)	$V_u/V_{u.cal}$
31		C-18-2	203.2	457.2	403.9	609.6	1.51	26.4	1.85	88.9	25.4	311.4	1.203
32		D-18-1	203.2	457.2	403.9	609.6	1.51	25.7	1.17	88.9	25.4	266.9	1.185
33		D-18-2	203.2	457.2	403.9	609.6	1.51	27.0	1.17	88.9	25.4	266.9	1.141
34		E-18-1	203.2	457.2	403.9	609.6	1.51	22.4	0.72	88.9	25.4	221.1	1.227
35		E-18-2	203.2	457.2	403.9	609.6	1.51	26.7	0.72	88.9	25.4	222.4	1.086
36	Leonhardt and	2	190.0	320.0	270.0	400.0	1.48	30.4	2.07	130.0	30	260.3	1.169
37	Walther (1962)	3	190.0	320.0	270.0	540.0	2.00	30.4	2.07	130.0	30	147.7	0.969
38	Mathey and	I-1	203.2	457.2	402.8	609.6	1.51	25.4	3.05	88.9	25.4	312.9	1.104
39	Watstein (1963)	I-2	203.2	457.2	402.8	609.6	1.51	23.0	3.05	88.9	25.4	310.7	1.180
40		II-3	203.2	457.2	402.8	609.6	1.51	21.9	1.88	88.9	25.4	261.8	1.162
41		II-4	203.2	457.2	402.8	609.6	1.51	26.4	1.88	88.9	25.4	312.9	1.207
42		III-5	203.2	457.2	402.8	609.6	1.51	25.7	1.85	88.9	25.4	288.5	1.139
43		III-6	203.2	457.2	402.8	609.6	1.51	25.6	1.85	88.9	25.4	290.7	1.152
44		IV-7	203.2	457.2	402.8	609.6	1.51	24.1	1.86	88.9	25.4	290.8	1.203
45		IV-8	203.2	457.2	402.8	609.6	1.51	24.9	1.86	88.9	25.4	304.0	1.228
46		V-9	203.2	457.2	402.8	609.6	1.51	23.1	1.16	88.9	25.4	224.0	1.080
47		V-10	203.2	457.2	402.8	609.6	1.51	27.0	1.16	88.9	25.4	268.4	1.154
48		VI-11	203.2	457.2	402.8	609.6	1.51	25.4	1.17	88.9	25.4	224.0	1.007
49		VI-12	203.2	457.2	402.8	609.6	1.51	25.7	1.17	88.9	25.4	268.4	1.198
50		V-13	203.2	457.2	402.8	609.6	1.51	22.4	0.75	88.9	25.4	222.4	1.227
51		V-14	203.2	457.2	402.8	609.6	1.51	26.7	0.75	88.9	25.4	224.0	1.089
52		VI-15	203.2	457.2	402.8	609.6	1.51	25.5	0.75	88.9	25.4	179.5	0.901
53		VI-16	203.2	457.2	402.8	609.6	1.51	22.8	0.75	88.9	25.4	188.6	1.028
54	Kani (1967)	46	151.1	152.4	135.9	271.8	2.00	25.5	2.76	88.9	19.05	69.0	1.025
55		53	151.1	152.4	132.1	135.6	1.03	26.7	2.84	88.9	19.05	155.2	1.015
56		54	151.1	152.4	135.9	135.6	1.00	26.7	2.76	88.9	19.05	157.7	0.998
57		67	157.2	609.6	528.3	542.5	1.03	30.3	2.75	88.9	19.05	547.8	1.253
58		69	155.2	609.6	542.3	542.5	1.00	27.4	2.67	88.9	19.05	585.4	1.411
59		3,041	152.4	1219.2	1097.3	2194.6	2.00	26.9	2.72	304.8	19.05	326.0	0.922
60	Manuel et al.	1	101.6	457.2	406.4	121.9	0.30	33.8	0.96	101.6	NR	445.0	1.310
61	(1971)	2	101.6	457.2	406.4	121.9	0.30	35.2	0.96	101.6	NR	445.1	1.279
62		3	101.6	457.2	406.4	121.9	0.30	30.1	0.96	101.6	NR	367.3	1.159
63		4	101.6	457.2	406.4	121.9	0.30	31.9	0.96	101.6	NR	400.8	1.219
64	Kani (1979)	24	152.4	304.8	271.3	406.9	1.50	27.9	1.87	88.9	19.05	181.9	1.192
65		25	152.4	304.8	271.3	542.5	2.00	24.6	1.87	88.9	19.05	104.1	1.067
66		26	152.4	304.8	271.3	542.5	2.00	27.1	1.87	88.9	19.05	78.1	0.745
67	Rogowsky et al. (1983)	BM1/1.5S	200.0	600.0	535.0	925.0	1.73	42.4	1.13	150.0	10	303.0	0.896
68	Mphonde and	AO-3-1	152.4	336.6	298.5	422.3	1.42	23.7	3.34	50.8	9.525	116.0	0.679
69	Frantz (1984)	AO-7-1	152.4	336.6	298.5	422.3	1.42	42.9	3.34	50.8	9.525	311.4	1.215
70		AO-15-1a	152.4	336.6	298.5	422.3	1.42	81.5	3.34	50.8	9.525	275.6	0.814
71	Kim and Park	A1.5-1	170.0	300.0	270.0	405.0	1.50	52.0	1.87	100.0	25	212.5	0.834
72	(1994)	A1.5-2	170.0	300.0	270.0	405.0	1.50	52.0	1.87	100.0	25	215.3	0.844
73	Scholz (1994)	B-1	200.0	400.0	368.0	736.0	2.00	84.5	2.00	100.0	16	298.7	0.938
74		C-1	200.0	400.0	366.0	732.0	2.00	83.9	3.36	100.0	16	352.7	0.972
75		D-1	200.0	400.0	362.0	724.0	2.00	96.8	1.94	100.0	16	307.7	0.981
76	Xie et al. (1994)	NNN-1	127.0	254.0	215.9	200.0	0.93	45.5	2.08	31.8	19.05	155.8	0.712
77		NNN-2	127.0	254.0	215.9	415.9	1.93	40.1	2.08	31.8	19.05	56.8	0.599
78		NHN-1	127.0	254.0	215.9	200.0	0.93	100.5	2.08	31.8	19.05	241.6	0.865
79		NHN-2	127.0	254.0	215.9	415.9	1.93	100.1	2.08	31.8	19.05	101.8	0.777
80	Walraven (1978)	V011	250.0	400.0	360.0	337.5	0.94	15.7	2.22	45.0	8	226.0	0.725
81		V012	250.0	400.0	360.0	337.5	0.94	21.2	2.22	45.0	8	322.0	0.820
82		V013	250.0	400.0	360.0	337.5	0.94	21.6	2.22	45.0	8	344.0	0.865
83		V014	250.0	400.0	360.0	337.5	0.94	23.7	2.22	45.0	8	425.0	0.996
84		V021	250.0	400.0	360.0	337.5	0.94	13.5	2.22	45.0	16	220.0	0.795
85		V022	250.0	400.0	360.0	335.0	0.93	19.4	1.13	50.0	16	270.0	0.868
86		V023	250.0	400.0	360.0	337.5	0.94	19.6	2.22	45.0	16	347.0	0.937
87		V024	250.0	400.0	360.0	337.5	0.94	24.5	2.22	45.0	16	396.0	0.906
88		V031	250.0	400.0	360.0	337.5	0.94	19.5	2.22	45.0	32	323.0	0.876
89		V032	250.0	400.0	360.0	337.5	0.94	17.7	2.22	45.0	32	318.0	0.927

Appendix II. (*Continued.*)

No.	Authors and reference	Specimen	b (mm)	h (mm)	d (mm)	a (mm)	a/d	f_c (MPa)	ρ (%)	l_{bt} (mm)	d_{ag} (mm)	V_u (kN)	$V_u/V_{u.cal}$
90		V033	250.0	400.0	360.0	337.5	0.94	19.3	2.22	45.0	32	246.0	0.671
91		V034	250.0	400.0	360.0	337.5	0.94	25.8	2.22	45.0	32	437.0	0.964
92	Walraven and	V511	250.0	600.0	560.0	522.5	0.93	19.3	1.12	75.0	16	350.0	0.793
93	Lehwalter	V411	250.0	800.0	740.0	690.0	0.93	18.9	1.10	100.0	16	365.0	0.672
94	(1994)	V211	250.0	1000.0	930.0	867.5	0.93	19.5	1.08	125.0	16	505.0	0.760
95	Foster and	B2.OB-5	125.0	700.0	624.0	762.5	1.22	89.0	2.42	125.0	10	585.9	1.053
96	Gilbert (1998)	B3.OB-5	125.0	700.0	624.0	1112.5	1.78	89.0	2.42	125.0	10	436.3	1.188
97	Tan et al. (1997)	1-1/0.75	110.0	500.0	462.5	375.0	0.81	56.3	2.47	150.0	10	500.9	1.017
98		II-1/1.00	110.0	500.0	462.5	500.0	1.08	77.6	2.47	150.0	10	256.0	0.576
99		III-l/1.50	110.0	500.0	462.5	750.0	1.62	77.6	2.47	150.0	10	186.2	0.639
100	Teng et al.	N-1a	150.0	600.0	525.0	862.5	1.64	38.2	1.93	75.0	NR	188.5	0.693
101	(1998)	N-1b	150.0	600.0	550.0	862.5	1.57	38.7	0.92	75.0	NR	206.0	0.830
102		N-1b(2)	160.0	600.0	550.0	862.5	1.57	38.1	0.86	75.0	NR	143.6	0.557
103		N1-1.5-WO	160.0	600.0	525.0	862.5	1.64	38.1	1.81	75.0	NR	161.1	0.565
104		N1-1.0-WO	160.0	600.0	525.0	562.5	1.07	38.4	1.81	75.0	NR	400.7	0.905
105	Tan and Lu	1-500/0,50	140.0	500.0	444.0	250.0	0.56	49.1	2.59	215.0	NR	426.1	0.561
106	(1999)	1-500/0,75	140.0	500.0	444.0	373.0	0.84	42.5	2.59	215.0	NR	351.2	0.636
107		1-500/1,00	140.0	500.0	444.0	500.0	1.13	37.4	2.59	215.0	NR	286.3	0.713
108	Oh and Shin	H4100	130.0	560.0	500.0	250.0	0.50	47.5	1.51	180.0	16	642.2	1.013
109	(2001)	H4200	130.0	560.0	500.0	425.0	0.85	47.5	1.51	180.0	16	401.1	0.822
110		H4500	130.0	560.0	500.0	935.0	1.87	47.5	1.51	180.0	16	112.5	0.504
111		H41A0	130.0	560.0	500.0	250.0	0.50	49.1	1.51	180.0	16	376.4	0.583
112		U41A0	130.0	560.0	500.0	250.0	0.50	71.3	1.51	180.0	16	474.5	0.633
113	Rosenbusch and Teutsch (2002)	2.2/1	200.0	300.0	260.0	375.0	1.44	40.3	1.81	50.0	NR	211.4	0.868
114	Yang et al.	L5-40	160.0	400.0	355.0	200.0	0.56	31.4	1.00	100.0	19	446.9	1.192
115	(2003)	L5-60	160.0	600.0	555.0	300.0	0.54	31.4	0.98	100.0	19	535.1	1.018
116		L5-60R	160.0	600.0	555.0	300.0	0.54	31.4	0.98	100.0	19	479.2	0.911
117		L5-75	160.0	750.0	685.0	375.0	0.55	31.4	1.00	100.0	19	596.8	0.966
118		L5-100	160.0	1000.0	935.0	500.0	0.54	31.4	0.90	100.0	19	582.1	0.760
119		L10-40	160.0	400.0	355.0	400.0	1.13	31.4	1.00	100.0	19	192.1	0.788
120		L10-40R	160.0	400.0	355.0	400.0	1.13	31.4	1.00	100.0	19	311.6	1.278
121		L10-60	160.0	600.0	555.0	600.0	1.08	31.4	0.98	100.0	19	375.3	1.077
122		L10-75	160.0	750.0	685.0	750.0	1.10	31.4	1.00	100.0	19	271.5	0.669
123		L10-75R	160.0	750.0	685.0	750.0	1.10	31.4	1.00	100.0	19	330.3	0.814
124		L10-100	160.0	1000.0	935.0	1000.0	1.07	31.4	0.90	100.0	19	543.9	1.066
125		UH5-40	160.0	400.0	355.0	200.0	0.56	78.5	1.00	100.0	19	733.0	1.252
126		UH5-60	160.0	600.0	555.0	300.0	0.54	78.5	0.98	100.0	19	823.2	0.997
127		UH5-75	160.0	750.0	685.0	375.0	0.55	78.5	1.00	100.0	19	1010.4	1.041
128		UH5-100	160.0	1000.0	935.0	500.0	0.54	78.5	0.90	100.0	19	1029.0	0.853
129		UH10-40	160.0	400.0	355.0	375.0	1.06	78.5	1.00	100.0	19	498.8	1.218
130		UH10-40R	160.0	400.0	355.0	375.0	1.06	78.5	1.00	100.0	19	385.1	0.940
131		UH10-60	160.0	600.0	555.0	600.0	1.08	78.5	0.98	100.0	19	573.3	1.031
132		UH10-75	160.0	750.0	685.0	750.0	1.10	78.5	1.00	100.0	19	338.1	0.522
133		UH10-75R	160.0	750.0	685.0	750.0	1.10	78.5	1.00	100.0	19	360.6	0.557
134		UH10-100	160.0	1000.0	935.0	1000.0	1.07	78.5	0.90	100.0	19	769.3	0.944
135	Tanimura and	1	300.0	450.0	400.0	200.0	0.50	23.2	2.20	100.0	NR	853.0	1.012
136	Sato (2005)	5	300.0	450.0	400.0	400.0	1.00	29.0	2.20	100.0	NR	632.0	0.982
137		9	300.0	450.0	400.0	600.0	1.50	22.9	2.20	100.0	NR	284.0	0.780
138		13	300.0	450.0	400.0	400.0	1.00	32.0	2.20	100.0	NR	661.0	0.960
139		24	300.0	450.0	400.0	200.0	0.50	79.9	2.20	100.0	NR	1958.0	1.216
140		25	300.0	450.0	400.0	400.0	1.00	76.4	2.20	100.0	NR	1403.0	1.303
141		26	300.0	450.0	400.0	600.0	1.50	78.3	2.20	100.0	NR	904.0	1.237
142		27	300.0	450.0	400.0	800.0	2.00	77.8	2.20	100.0	NR	752.0	1.467
143		35	300.0	450.0	400.0	200.0	0.50	25.3	0.44	100.0	NR	588.0	1.103
144		38	300.0	450.0	400.0	400.0	1.00	25.2	0.44	100.0	NR	358.0	0.947
145	Quintero-Febres	A3	150.0	460.0	370.0	499.3	1.35	21.3	2.74	98.5	10	221.4	1.147
146	et al. (2006)	A4	150.0	460.0	370.0	499.3	1.35	21.3	2.74	98.5	10	196.4	1.018
147		B3	150.0	460.0	375.0	291.0	0.78	31.4	2.02	121.9	10	468.2	1.197
148		B4	150.0	460.0	375.0	291.0	0.78	31.4	2.02	121.9	10	459.2	1.174

J. Struct. Eng., 2023, 149(11): 04023159

Appendix II. (*Continued.*)

No.	Authors and reference	Specimen	b (mm)	h (mm)	d (mm)	a (mm)	a/d	f_c (MPa)	ρ (%)	l_{bt} (mm)	d_{ag} (mm)	V_u (kN)	$V_u/V_{u.cal}$
149		HA3	150.0	460.0	380.0	519.9	1.37	48.7	2.67	99.8	10	292.4	0.870
150		HB3	150.0	460.0	380.0	295.7	0.78	48.7	2.67	121.5	10	460.2	0.825
151	Zhang and Tan (2007)	2DB35	80.0	350.0	314.0	350.0	1.12	27.4	1.25	52.5	10	85.0	0.830
152		2DB50	80.0	500.0	459.0	500.0	1.09	32.4	1.18	75.0	10	135.5	0.858
153		2DB70	80.0	700.0	650.0	700.0	1.08	24.8	1.33	105.0	10	155.5	0.860
154		2DB100	80.0	1000.0	926.0	1000.0	1.08	30.6	1.30	150.0	10	241.5	0.870
155		3DB35b	80.0	350.0	314.0	350.0	1.12	27.4	1.25	52.5	10	85.0	0.830
156		3DB50b	115.0	500.0	454.0	500.0	1.10	28.3	1.28	75.0	10	167.0	0.804
157		3DB70b	160.0	700.0	642.0	700.0	1.09	28.7	1.22	105.0	10	360.5	0.937
158		3DB100b	230.0	1000.0	904.0	1000.0	1.11	29.3	1.20	150.0	10	672.0	0.922
159	Birrcher et al. (2009)	III-1.85-00	533.4	1066.8	980.4	1617.8	1.65	21.2	2.31	371.3	19.05	1621.6	1.353
160	Tanaka et al. (2010)	No.1_B2-1.0	50.0	225.0	200.0	200.0	1.00	21.5	0.64	50.0	25	48.0	1.388
161		No.2_B4-1.0	100.0	450.0	400.0	400.0	1.00	27.7	0.62	100.0	25	226.0	1.527
162		No.3_B8-1.0	200.0	900.0	800.0	800.0	1.00	25.7	0.64	200.0	25	685.0	1.372
163		No.7_B2-1.5	50.0	225.0	200.0	300.0	1.50	36.8	0.64	50.0	25	36.0	1.087
164		No.8_B4-1.5	100.0	450.0	400.0	600.0	1.50	33.6	0.62	100.0	25	114.0	0.996
165		No.9_B8-1.5	200.0	900.0	800.0	1200.0	1.50	26.9	0.64	200.0	25	258.0	0.736
166	Mihaylov et al. (2010)	S0M	400.0	1200.0	1094.0	1625.0	1.49	34.2	0.70	150.0	20	721.0	0.681
167		S0C	400.0	1200.0	1094.0	1625.0	1.49	34.2	0.70	150.0	20	1162.0	1.098
168	El-Sayed and Shuraim (2016)	B350-1-30	150.0	350.0	293.0	293.0	1.00	26.1	1.40	58.6	20	203.5	1.012
169		B500-1-30	150.0	500.0	419.0	419.0	1.00	26.1	1.47	83.8	20	234.5	0.858
170		B700-1-30	150.0	700.0	615.0	615.0	1.00	26.1	1.44	123.0	20	453.0	1.220
171		B1000-1-30	150.0	1000.0	910.0	910.0	1.00	26.1	1.47	182.0	20	546.0	1.065
172		B350-1-55	150.0	350.0	293.0	293.0	1.00	53.9	1.40	58.6	20	380.0	1.204
173		B500-1-55	150.0	500.0	419.0	419.0	1.00	53.9	1.47	83.8	20	415.5	0.966
174		B700-1-55	150.0	700.0	615.0	615.0	1.00	53.9	1.44	123.0	20	590.0	1.008
175		B1000-1-55	150.0	1000.0	910.0	910.0	1.00	53.9	1.47	182.0	20	742.5	0.919
176		B350-1-75	150.0	350.0	293.0	293.0	1.00	70.1	1.40	58.6	20	389.5	1.107
177		B500-1-75	150.0	500.0	419.0	419.0	1.00	70.1	1.47	83.8	20	440.5	0.917
178		B700-1-75	150.0	700.0	615.0	615.0	1.00	70.1	1.44	123.0	20	770.5	1.179
179		B1000-1-75	150.0	1000.0	910.0	910.0	1.00	70.1	1.47	182.0	20	810.0	0.896
180	Li et al. (2021)	D180-C35	200.0	210.0	180.0	160.0	0.89	30.3	1.80	40.0	21.5	273.9	1.170
181		D360-C35	200.0	400.0	360.0	320.0	0.89	28.6	1.80	80.0	21.5	399.9	0.998
182		D720-C35	200.0	800.0	720.0	640.0	0.89	27.4	1.80	160.0	21.5	802.0	1.176
183		D1440-C35	200.0	1600.0	1440.0	1280.0	0.89	31.5	1.80	320.0	21.5	1544.0	1.165
184		D180-C50	200.0	207.0	180.0	160.0	0.89	41.6	1.80	40.0	21.5	307.3	1.069
185		D360-C50	200.0	400.0	360.570	320.0	0.89	38.2	1.80	80.0	21.5	561.1	1.155
186		D720-C50	200.0	800.0	720.0	640.0	0.89	41.0	1.80	160.0	21.5	1148.7	1.289
187		D1440-C50	200.0	1600.0	1440.0	1280.0	0.89	43.3	1.80	320.0	21.5	1851.0	1.142
188	Li et al. (2022)	SL2_200_1	200.0	200.0	170.0	320.0	1.88	41.6	1.80	40.0	21.5	196.5	1.571
189		SL2_400_1	200.0	400.0	360.0	680.0	1.89	39.5	1.80	80.0	21.5	175.5	0.761
190		SL2_800_1	200.0	800.0	720.0	1360.0	1.89	35.5	1.80	160.0	21.5	456.5	1.199
191		SL2_1600_1	200.0	1600.0	1440.0	2720.0	1.89	38.9	1.80	320.0	21.5	540.5	0.762
192		SL2_200_2	200.0	200.0	170.0	320.0	1.88	27.0	1.80	40.0	21.5	171.0	1.804
193		SL2_400_2	200.0	400.0	360.0	680.0	1.89	24.8	1.80	80.0	21.5	170.0	1.011
194		SL2_800_2	200.0	800.0	720.0	1360.0	1.89	26.5	1.80	160.0	21.5	493.0	1.582

Note: NR = not reported; and $V_u/V_{u,cal}$ = the shear strength ratio calculated by the proposed model in this paper.

Data Availability Statement

All data, models, and code generated or used during the study appear in the published article.

Acknowledgments

The authors gratefully acknowledge the financial support provided by the National Natural Science Foundation of China (Nos. 51878260 and 52078201) and the Hunan Provincial Innovation Foundation for Postgraduate No. 541109080046 (CX2017B121). The findings and opinions expressed in this paper are those of the authors and do not necessarily reflect those of the sponsor.

Notation

The following symbols are used in this paper:

a = shear span length;

b = width of beam section;

C_1–C_4 = undetermined parameters;
c = distance from extreme compression fiber to the flexural neutral axis;
c' = depth of uncracked concrete at the edge of the loading plate;
d = effective depth of beam section;
d_{ag} = maximum aggregate size;
d_b = diameter of longitudinal reinforcement;
E_c = concrete elastic modulus;
E_s = steel elastic modulus;
F_{str} = ultimate resultant force in the strut;
f_c = cylinder compressive strength of concrete;
f_{cu} = cubic compressive strength of concrete;
f_y = yield stress of longitudinal reinforcement;
h = beam height;
l_{bt} = length of the loading plate;
l_c = length of the whole critical shear crack;
l_{de} = length of delamination crack;
n = ratio of steel elastic modulus to the concrete elastic modulus;
n_b = number of longitudinal reinforcement;
s = crack sliding;
V = shear force;
V_{ag} = shear force carried by aggregate interlock;
$V_{ag,BD}$ = aggregate interlock force along the crack surface BD;
V_{cal} = shear strength predicted by shear models;
$V_{cn,AB}$, $V_{cn,CD}$ = shear forces in the cross section AB and CD, respectively;
V_d = shear force carried by dowel action;
V_u = ultimate shear strength of beams;
w = crack width;
w_{str} = width of the top of the uncracked concrete strut;
α = azimuth angle;
$\alpha_c(t)$ = inclination angle of each crack segment;
Δl_r = elongation of longitudinal reinforcement along the length of the beam;
η = coefficient taking account of the contribution of aggregate interlock and dowel action to shear capacity;
θ = angle between the center line of the strut and the horizontal direction;
κ = brittleness coefficient;
ξ = size effect factor;
ξ_{exp} = experimental value of the size effect factor;
ρ = ratio of the longitudinal reinforcement;
Σw_i = sum of crack widths at 1/4 height of the beam;
σ_{ag}, τ_{ag} = normal and shear stress on the crack surface due to aggregate interlock, respectively;
σ_{sc} = tensile stress in longitudinal reinforcement;
σ_1, σ_2 = principal stresses;
τ_m = shear stress; and
ϕ = strength reduction factor.

References

AASHTO. 2017. *Bridge design specifications*. Washington, DC: AASHTO.

ACI (American Concrete Institute). 2019. *Building code requirements for structural concrete: Commentary on building code requirements for structural concrete*. Farmington Hills, MI: ACI.

Bažant, Z. 1984. "Size effect in blunt fracture: Concrete, rock, metal." *J. Eng. Mech.* 110 (4): 518–535. https://doi.org/10.1061/(ASCE)0733-9399(1984)110:4(518).

Bažant, Z. P., and M. T. Kazemi. 1991. "Size effect on diagonal shear failure of beams without stirrups." *ACI Struct. J.* 88 (3): 268–276. https://doi.org/10.14359/3097.

Bažant, Z. P., and J. K. Kim. 1984. "Size effect in shear failure of longitudinally reinforced beams." *ACI J. Proc.* 81 (5): 456–468. https://doi.org/10.14359/10696.

Bažant, Z. P., Q. Yu, W. Gerstle, J. Hanson, and J. W. Ju. 2007. "Justification of ACI 446 proposal for updating ACI code provisions for shear design of reinforced concrete beams." *Struct. J.* 104 (5): 601–610. https://doi.org/10.14359/18862.

Bažant, Z. P., Q. Yu, M. H. Hubler, V. Krístek, and Z. Bittnar. 2011. "Wake-up call for creep, myth about size effect and black holes in safety: What to improve in fib model code draft." In *Proc., fib Symp. PRAGUE 2011: Concrete Engineering for Excellence and Efficiency*, 731–746. Prague, Czech Republic: Czech Concrete Society.

Bentz, E. C. 2005. "Empirical modeling of reinforced concrete shear strength size effect for members without stirrups." *ACI Struct. J.* 102 (2): 232. https://doi.org/10.14359/14274.

Bentz, E. C., and M. P. Collins. 2018. "The Toronto size effect series." *Spec. Publ.* 328 (Sep): 1–12. https://doi.org/10.14359/51711146.

Bentz, E. C., F. J. Vecchio, and M. P. Collins. 2006. "Simplified modified compression field theory for calculating shear strength of reinforced concrete elements." *ACI Struct. J.* 103 (4): 614. https://doi.org/10.14359/16438.

Birrcher, D., R. Tuchscherer, M. Huizinga, O. Bayrak, S. Wood, and J. Jirsa. 2009. *Strength and serviceability design of reinforced concrete deep beams*. Austin, TX: Univ. of Texas.

Brown, M. D., and O. Bayrak. 2008a. "Design of deep beams using strut-and-tie models—Part I: Evaluating U.S. provisions." *ACI Struct. J.* 105 (4): 395–404. https://doi.org/10.14359/19853.

Brown, M. D., and O. Bayrak. 2008b. "Design of deep beams using strut-and-tie models—Part II: Design recommendations." *ACI Struct. J.* 105 (4): 405–413. https://doi.org/10.14359/19854.

CEB-FIP MC (Euro-International Committee for Concrete-International Federation for Prestressing Model Code). 2010. *fib model code for concrete structures 2010*. Berlin: Ernst & Sohn.

CEN (European Committee for Standardization). 2004. *Design of concrete structures—Part 1-1: General rules and rules for buildings*. Brussels, Belgium: CEN.

Chen, H., W.-J. Yi, and H.-J. Hwang. 2018. "Cracking strut-and-tie model for shear strength evaluation of reinforced concrete deep beams." *Eng. Struct.* 163 (May): 396–408. https://doi.org/10.1016/j.engstruct.2018.02.077.

China Architectural and Building Press. 2010. *Code for design of concrete structures*. GB50010-2010. Beijing: China Architectural and Building Press.

Choi, K.-K., H.-G. Park, and J. K. Wight. 2007. "Unified shear strength model for reinforced concrete beams—Part I: Development." *ACI Struct. J.* 104 (2): 142–152. https://doi.org/10.14359/18526.

Cladera, A., A. Marí, J.-M. Bairán, E. Oller, and C. Ribas. 2017. "One-way shear design method based on a multi-action model." *Concr. Int.* 39 (9): 40–46.

Clark, A. P. 1951. "Diagonal tension in reinforced concrete beams." *J. Proc.* 48 (10): 145–156. https://doi.org/10.14359/11876.

Collins, M. P., E. C. Bentz, P. T. Quach, and G. T. Proestos. 2015. "The challenge of predicting the shear strength of very thick slabs." *Concr. Int.* 37 (11): 29–37.

Collins, M. P., and D. Kuchma. 1999. "How safe are our large, lightly reinforced concrete beams, slabs, and footings?" *ACI Struct. J.* 96 (4): 482–491. https://doi.org/10.14359/684.

CSA (Canadian Standards Association). 2014. *Design of concrete structures*. Toronto: CSA.

Daluga, D., K. McCain, M. Murray, and S. Pujol. 2018. "Effect of geometric scaling on shear strength of reinforced concrete beams without stirrups." *ACI Struct. J.* 115 (1): 1813–1815. https://doi.org/10.14359/51700947.

J. Struct. Eng., 2023, 149(11): 04023159

El-Sayed, A. K., and A. B. Shuraim. 2016. "Size effect on shear resistance of high strength concrete deep beams." *Mater. Struct.* 49 (5): 1871–1882. https://doi.org/10.1617/s11527-015-0619-1.

Foster, S. J., and R. I. Gilbert. 1998. "Experimental studies on high-strength concrete deep beams." *ACI Struct. J.* 95 (4): 382–390. https://doi.org/10.14359/554.

Hwang, S.-J., W.-Y. Lu, and H.-J. Lee. 2000. "Shear strength prediction for deep beams." *ACI Struct. J.* 97 (3): 367–376. https://doi.org/10.14359/9624.

Kani, G. N. J. 1967. "How safe are our large reinforced concrete beams." *ACI J.* 64 (12): 128–141. https://doi.org/10.14359/7549.

Kani, G. N. J. 1979. *Kani on shear in reinforced concrete*. Toronto: Univ. of Toronto.

Kim, J.-K., and S.-H. Eo. 1990. "Size effect in concrete specimens with dissimilar initial cracks." *Mag. Concr. Res.* 42 (153): 233–238. https://doi.org/10.1680/macr.1990.42.153.233.

Kim, J.-K., and Y.-D. Park. 1994. "Shear strength of reinforced high strength concrete beam without web reinforcement." *Mag. Concr. Res.* 46 (166): 7–16. https://doi.org/10.1680/macr.1994.46.166.7.

Korol, E., J. Tejchman, and Z. Mróz. 2017. "Experimental and numerical assessment of size effect in geometrically similar slender concrete beams with basalt reinforcement." *Eng. Struct.* 141 (Jun): 272–291. https://doi.org/10.1016/j.engstruct.2017.03.011.

Kotsovos, M. D. 1988. "Compressive force path concept: Basis for reinforced concrete ultimate limit state design." *ACI Struct. J.* 85 (1): 68–75. https://doi.org/10.14359/2986.

Lemaitre, J. 1971. *Evaluation of dissipation and damage in metals submitted to dynamic loading*. Kyoto, Japan: ICM.

Leonhardt, F., and R. Walther. 1962. "Beiträge zur Behandlung der Schubprobleme in Stahlbetonbau." *J. Beton-Und Stahlbetonbau* 7: 161–173.

Lesley, H. S., and A. R. Julio. 2010. "Influence of effective depth on shear strength of concrete beams—Experimental study." *ACI Struct. J.* 107 (5): 554–562. https://doi.org/10.14359/51663906.

Li, J., and X. Ren. 2009. "Stochastic damage model for concrete based on energy equivalent strain." *Int. J. Solids Struct.* 46 (11): 2407–2419. https://doi.org/10.1016/j.ijsolstr.2009.01.024.

Li, Y., H. Chen, W.-J. Yi, F. Peng, Z. Li, and Y. Zhou. 2021. "Effect of member depth and concrete strength on shear strength of RC deep beams without transverse reinforcement." *Eng. Struct.* 241 (Aug): 112427. https://doi.org/10.1016/j.engstruct.2021.112427.

Li, Y., Z. Li, W.-J. Yi, H. Chen, and W.-X. Zhang. 2022. "Study on size effect in shear strength of reinforced concrete short beams without stirrups." *China Civ. Eng. J.* 55 (12): 1–12. https://doi.org/10.15951/j.tmgcxb.21111100.

Lubell, A., T. Sherwood, E. Bentz, and M. P. Collins. 2004. "Safe shear design of large wide beams." *Concr. Int.* 26 (1): 67–78.

Manuel, R. F., B. W. Slight, and G. T. Suter. 1971. "Deep beam behavior affected by length and shear span variations." *ACI J. Proc.* 68 (12): 954–958.

Matamoros, A. B., and K. H. Wong. 2003. "Design of simply supported deep beams using strut-and-tie models." *ACI Struct. J.* 100 (6): 704–712. https://doi.org/10.14359/12836.

Mathey, R. G., and D. Watstein. 1963. "Shear strength of beams without web reinforcement containing deformed bars of different yield strengths." *ACI J. Proc.* 60 (2): 183–203. https://doi.org/10.14359/7851.

Mihaylov, B. I., E. C. Bentz, and P. C. Michael. 2010. "Behavior of large deep beams subjected to monotonic and reversed cyclic shear." *ACI Struct. J.* 107 (6): 726–734. https://doi.org/10.14359/51664021.

Mihaylov, B. I., E. C. Bentz, and P. C. Michael. 2013. "Two-parameter kinematic theory for shear behavior of deep beams." *ACI Struct. J.* 110 (3): 448–456. https://doi.org/10.14359/51685602.

Moody, K. G., I. M. Viest, R. C. Elstner, and E. Hognestad. 1954. "Shear strength of RC beams: Part 1—Tests of simple beams." *ACI J. Proc.* 51 (12): 317–332.

Morrow, J., and I. M. Viest. 1957. "Shear strength of reinforced concrete frame members without web reinforcement." *ACI J. Proc.* 53 (3): 833–869. https://doi.org/10.14359/11558.

Mphonde, A. G., and G. C. Frantz. 1984. "Shear tests of high- and low-strength concrete beams without stirrups." *ACI J. Proc.* 81 (4): 350–357. https://doi.org/10.14359/10690.

Oh, J.-K., and S.-W. Shin. 2001. "Shear strength of reinforced high-strength concrete deep beams." *ACI Struct. J.* 98 (2): 164–173. https://doi.org/10.14359/10184.

Park, H.-G., S. Kang, and K.-K. Choi. 2013. "Analytical model for shear strength of ordinary and prestressed concrete beams." *Eng. Struct.* 46 (Jan): 94–103. https://doi.org/10.1016/j.engstruct.2012.07.015.

Quintero-Febres, C. G., G. Parra-Montesinos, and J. K. Wight. 2006. "Strength of struts in deep concrete members designed using strut-and-tie method." *ACI Struct. J.* 103 (4): 577. https://doi.org/10.14359/16434.

Reineck, K.-H., D. A. Kuchma, K. S. Kim, and S. Marx. 2003. "Shear database for reinforced concrete members without shear reinforcement." *ACI Struct. J.* 100 (2): 240–249. https://doi.org/10.14359/12488.

Reineck, K.-H., and L. Todisco. 2014. "Database of shear tests for non-slender reinforced concrete beams without stirrups." *ACI Struct. J.* 111 (6): 1363–1372. https://doi.org/10.14359/51686820.

Rogowsky, D. M., J. G. MacGregor, and S. Y. Ong. 1983. *Tests of reinforced concrete deep beams*. Edmonton, AB, Canada: Univ. of Alberta.

Rosenbusch, J., and M. Teutsch. 2002. "Trial beams in shear." In *Brite Durham project*, 97. Braunschweig, Germany: Univ. of Braunschweig.

Russo, G., R. Venir, and M. Pauletta. 2005. "Reinforced concrete deep beams–Shear strength model and design formula." *ACI Struct. J.* 102 (3): 429–437. https://doi.org/10.14359/14414.

Scholz, H. 1994. *Ein Querkrafttragmodell für Bauteile ohne Schubbewehrung im Bruchzustand aus normalfestem und hochfestem Beton*. Berlin: Univ. bibliothek.

Shioya, T., M. Iguro, Y. Nojiri, H. Akiyama, and T. Okada. 1990. "Shear strength of large reinforced concrete beams." *Spec. Publ.* 118 (Jan): 259–280. https://doi.org/10.14359/2978.

Tan, K. H., and G. H. Cheng. 2006. "Size effect on shear strength of deep beams: Investigating with strut-and-tie model." *J. Struct. Eng.* 132 (5): 673–685. https://doi.org/10.1061/(ASCE)0733-9445(2006)132:5(673.

Tan, K. H., and H. Y. Lu. 1999. "Shear behavior of large reinforced concrete deep beams and code comparisons." *ACI Struct. J.* 96 (5): 836–845. https://doi.org/10.14359/738.

Tan, K. H., C. Y. Tang, and K. Tong. 2003. "A direct method for deep beams with web reinforcement." *Mag. Concr. Res.* 55 (1): 53–63. https://doi.org/10.1680/macr.2003.55.1.53.

Tan, K. H., K. Tong, and C. Y. Tang. 2001. "Direct strut-and-tie model for prestressed deep beams." *J. Struct. Eng.* 127 (9): 1076–1084. https://doi.org/10.1061/(ASCE)0733-9445(2001)127:9(1076.

Tan, K.-H., F.-K. Kong, S. Teng, and L.-W. Weng. 1997. "Effect of web reinforcement on high-strength concrete deep beams." *ACI Struct. J.* 94 (5): 573–581. https://doi.org/10.14359/506.

Tanaka, Y., T. Shimomura, and M. Watanabe. 2010. "Role of diagonal tension crack in size effect of shear strength of deep beams." In *Proc., Framcos-7*, 198–206. Seoul: Korea Concrete Institute.

Tanimura, Y., and T. Sato. 2005. "Evaluation of shear strength of deep beams with stirrups." *Q. Rep. RTRI* 46 (1): 53–58. https://doi.org/10.2219/rtriqr.46.53.

Teng, S., F. Kong, and S. Poh. 1998. "Shear strength of reinforced and prestressed concrete deep beams. Part II: The supporting evidence." *Proc. Inst. Civ. Eng. Struct. Build.* 128 (2): 124–143. https://doi.org/10.1680/istbu.1998.30120.

Trandafir, A. N., G. T. Proestos, and B. I. Mihaylov. 2022. "Detailed crack-based assessment of a 4-m deep beam test specimen." *Struct. Concr.* 24 (1): 756–770. https://doi.org/10.1002/suco.202200149.

Tureyen, A. K., and R. J. Frosch. 2003. "Concrete shear strength: Another perspective." *ACI Struct. J.* 100 (5): 609–615. https://doi.org/10.14359/12802.

Vecchio, F. J., and M. P. Collins. 1986. "The modified compression-field theory for reinforced concrete elements subjected to shear." *ACI J. Proc.* 83 (2): 219–231. https://doi.org/10.14359/10416.

Walraven, J. 1980. *Aggregate interlock: A theoretical and experimental analysis*. Delft, Netherlands: Delft Univ. of Technology.

Walraven, J., and N. Lehwalter. 1994. “Size effects in short beams loaded in shear.” *ACI Struct. J.* 91 (5): 585–593. https://doi.org/10.14359/4177.

Walraven, J. C. 1978. *Influence of member depth on the shear strength of lightweight concrete beams without shear reinforcement*. Rep. No. 5-78-4. Delft, Netherlands: Delft Univ. of Technology.

Watstein, D., and R. G. Mathey. 1958. “Strains in beams having diagonal cracks.” *ACI J. Proc.* 55 (12): 717–728. https://doi.org/10.14359/11384.

Wight, J. K., and J. G. MacGregor. 2011. *Reinforced concrete mechanics and design*. Upper Saddle River, NJ: Pearson.

Wu, J. Y., J. Li, and R. Faria. 2006. “An energy release rate-based plastic-damage model for concrete.” *Int. J. Solids Struct.* 43 (3): 583–612. https://doi.org/10.1016/j.ijsolstr.2005.05.038.

Xie, Y., S. H. Ahmad, T. Yu, S. Hino, and W. Chung. 1994. “Shear ductility of reinforced concrete beams of normal and high-strength concrete.” *ACI Struct. J.* 91 (2): 140–149. https://doi.org/10.14359/4592.

Yang, K.-H., and A. F. Ashour. 2011. “Strut-and-tie model based on crack band theory for deep beams.” *J. Struct. Eng.* 137 (10): 1030–1038. https://doi.org/10.1061/(ASCE)ST.1943-541X.0000351.

Yang, K.-H., H.-S. Chung, E.-T. Lee, and H.-C. Eun. 2003. “Shear characteristics of high-strength concrete deep beams without shear reinforcements.” *Eng. Struct.* 25 (10): 1343–1352. https://doi.org/10.1016/S0141-0296(03)00110-X.

Yu, Q., J. L. Le, M. H. Hubler, R. Wendner, G. Cusatis, and Z. P. Bažant. 2016. “Comparison of main models for size effect on shear strength of reinforced and prestressed concrete beams.” *Struct. Concr.* 17 (5): 778–789. https://doi.org/10.1002/suco.201500126.

Zararis, P. D., and G. C. Papadakis. 2001. “Diagonal shear failure and size effect in RC beams without web reinforcement.” *J. Struct. Eng.* 127 (7): 733–742. https://doi.org/10.1061/(ASCE)0733-9445(2001)127:7(733).

Zhang, N., and K. H. Tan. 2007. “Size effect in RC deep beams: Experimental investigation and STM verification.” *Eng. Struct.* 29 (12): 3241–3254. https://doi.org/10.1016/j.engstruct.2007.10.005.